1

Advancements in Urology 2024
COI Disclosure Information
Gaku Yamamichi
We have no COI with regard to our presentation.

GDF15 propeptide is a novel blood biomarker for castration-resistant prostate cancer patients with bone metastasis via promoting the vicious cycle

Gaku Yamamichi[1], Taigo Kato[1], Yuichi Motoyama[2], Hidetatsu Outani[3], Shohei Myoba[4], Noriaki Arakawa[5], Masaru Tani[1], Akihiro Yoshimura[1], Yohei Okuda[1]
Yu Ishizuya[1], Yoshiyuki Yamamoto[1], Koji Hatano[1], Atsunari Kawashima[1], Takeshi Ujike[1], Motohide Uemura[6,7], Norio Nonomura[1]
1:Department of Urology, Osaka University Graduate School of Medicine 2:Department of Pathology, Osaka University Graduate School of Medicine 3:Department of Orthopedic Surgery, Osaka University Graduate School of Medicine 4:Bioscience Division, Research and Development Department, Tosoh Corporation 5: Division of Medical Safety Science, National Institute of Health Science 6:Department of Urology, Iwase General Hospital 7:Department of Urology Fukushima Medical University

Grant support
This work was supported by KAKENHI grant (21K09396 and 20K23002)

Background and objectives

Bone metastasis (BM) occurs in 90% of advanced castration-resistant prostate cancer (CRPC) and no blood marker is useful for BM. Bone scan index (BSI) is relatively accurate for BM and represents BM status but there are few facilities where BSI measure. In this study, we aimed to discover the novel blood biomarker for diagnosis and monitoring BM and elucidate its clinical utility and mechanism involved in bone turnover.

Conclusions

Secretome analysis revealed GDPP was secreted by PC cell, osteoblast and osteoclast. *In vitro* and *in vivo*, we found GDPP not only promoted CRPC progression, but also increased the bone-forming and bone-resorbing ability in BM microenvironment. In CRPC patients with BM, GDPP correlated more strongly with BSI than PSA and other blood biomarkers, indicating GDPP might be a novel diagnostic and monitoring biomarker.

Vicious cycle of bone metastasis and clinical application of GDPP

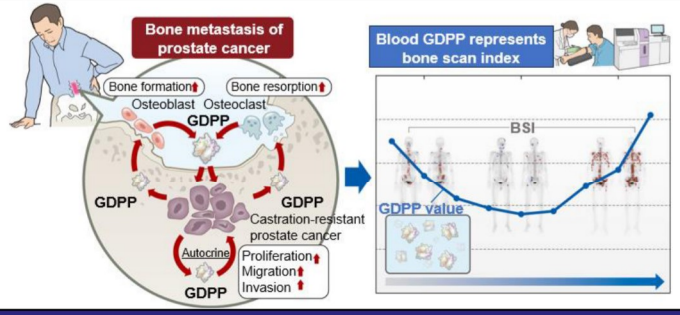

Materials and methods

Cell lines: 7 PC 4 RCC 4 BC

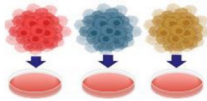

Supernatant

Orbitrap LC-MS (Thermo Scientific)

Secretome analysis

① PC cell lines specific proteins
② Secreted or membrane proteins (GO analysis)
③ Proteins with no reports as biomarkers

Functional analysis in bone microenvironment

① We comprehensively evaluated secreted proteins from 15 types of cell lines to identify proteins, specifically secreted by PC cells.
② *In vitro and vivo*, we examined its functions of the protein using CRPC cell lines (PC3 and DU145), human osteoblast and osteoclast.
③ *In clinical settings*, we analyzed the utility of this blood biomarker.

CRPC cell
Osteoblast
Osteoclast

BM model

Results

1. Discovery of the target protein by secretome analysis

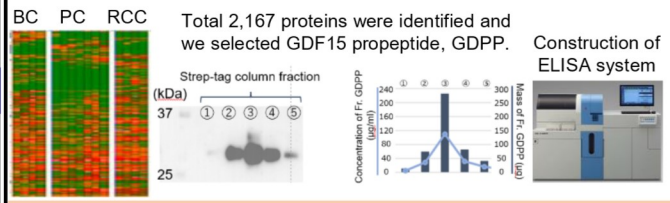

➢ **GDPP was identified as novel biomarker by secretome analysis and recombinant GDPP was purified and ELISA system was established**

2. Molecular dynamics of GDPP inside and outside the cell

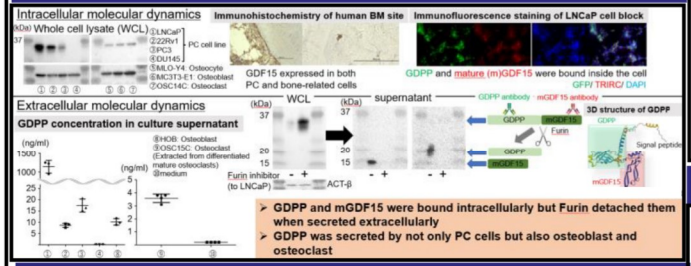

➢ **GDPP and mGDF15 were bound intracellularly but Furin detached them when secreted extracellularly**
➢ **GDPP was secreted by not only PC cells but also osteoblast and osteoclast**

3. Function of GDPP in CRPC cell lines

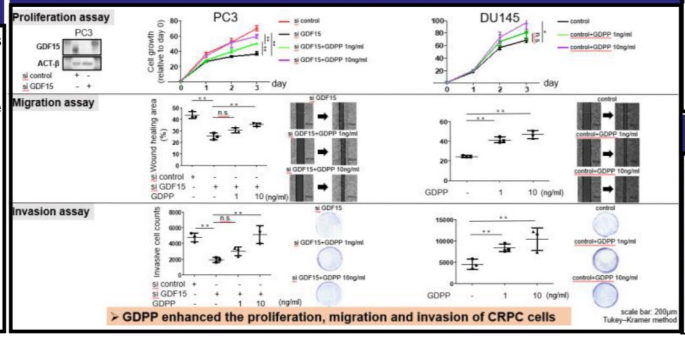

➢ **GDPP enhanced the proliferation, migration and invasion of CRPC cells**

4. Function of GDPP in osteoblast (HOB) and osteoclast (OSC15C)

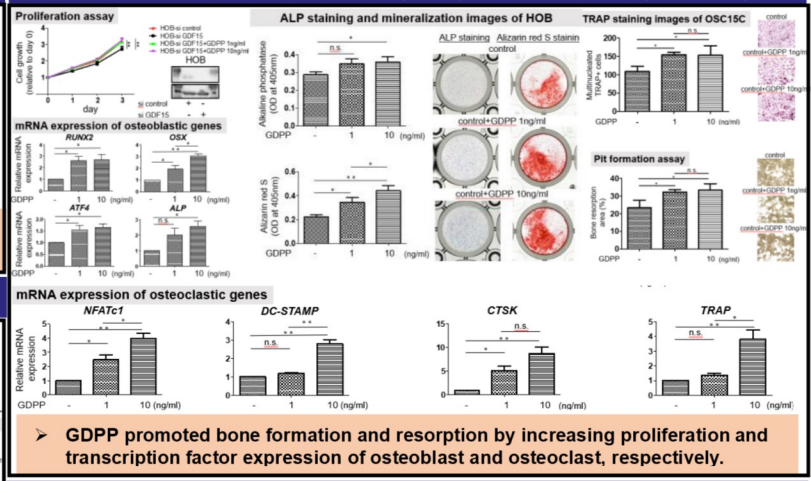

➢ **GDPP promoted bone formation and resorption by increasing proliferation and transcription factor expression of osteoblast and osteoclast, respectively.**

5. Function of GDPP in bone metastasis mouse model

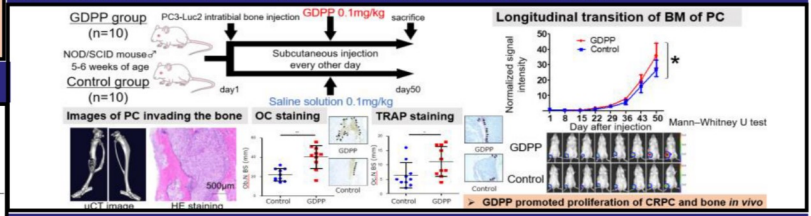

➢ **GDPP promoted proliferation of CRPC and bone *in vivo***

6. Plasma GDPP as a blood biomarker of BM in CRPC patients

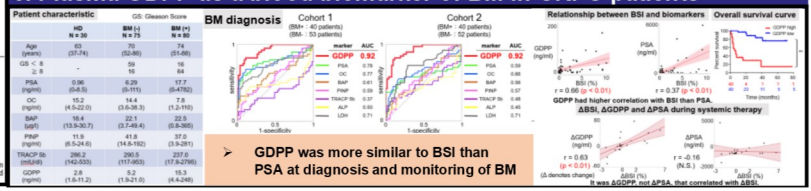

➢ **GDPP was more similar to BSI than PSA at diagnosis and monitoring of BM**

2

Impact of Thienopyridine Class Antiplatelets on Bleeding Outcomes Following Robot-Assisted Radical Prostatectomy: A Cohort Study from a Multicenter Database

[1]Takayuki Goto, [1,2]Masashi Kubota, [2]Mutsushi Kawakita, [1]Takayuki Sumiyoshi, , [3]Ryoma Kurahashi, [4]Kimihiro Shimatani, [5]Yuya Sekine, [6]Hiromitsu Negoro, [7]Atsuro Sawada, [8]Shusuke Akamatsu, [1]Takashi Kobayashi

[1]Department of Urology, Kyoto University Graduate School of Medicine, Kyoto, Japan. [2]Department of Urology, Kobe City Medical Center General Hospital, Hyogo, Japan. [3]Department of Urology, Faculty of Life Sciences, Kumamoto University, Kumamoto, Japan. [4]Department of Urology, Hyogo Medical University, Nishinomiya, Hyogo, Japan. [5]Department of Urology, Akita University Graduate School of Medicine, Akita, Japan. [6]Department of Urology, University of Tsukuba, Tsukuba, Ibaraki, Japan. [7]Department of Urology, Nagoya University, Aichi, Japan. [8]Department of Urology, Miyazaki University, Miyazaki, Japan.

PURPOSE

This study aims to evaluate the effects of thienopyridine-class antiplatelet agents, including ticlopidine, clopidogrel, and prasugrel, on bleeding complications in patients who underwent robot-assisted radical prostatectomy.

METHODS

This cohort study used a database for robot-assisted radical prostatectomy at 23 tertiary centers nationwide. Among 7700 patients who underwent RARP between 2011 and 2022, patients who received thienopyridines (thienopyridine group) were compared with those who received aspirin monotherapy (aspirin group). The primary outcome focused on the incidence of bleeding complications that required transfusion, additional intervention, or readmission. High-grade complications were defined as Clavien–Dindo grade III or higher. The characteristics of the two groups were adjusted using inverse probability of treatment weighting with propensity scores. The risks of these outcomes were evaluated using weighted regression models.

RESULTS

This study included 520 patients, with 147 in the thienopyridine group and 373 in the aspirin group, respectively. Within the thienopyridine group, 126 (86%) received clopidogrel and 52 (35%) received dual antiplatelet therapy. Thienopyridine therapy was associated with a higher risk of bleeding complications (OR:3.62, 95%CI:1.548.49), transfusion (OR:6.35, 95%CI:1.75–23.0), and readmission (OR:2.96, 95%CI:1.346.54). The increased risks of the thienopyridine group were detected for low-grade bleeding complications (OR:3.20, 95%CI:1.23–8.30) but not for high-grade bleeding complications (OR:5.23, 95%CI:0.78–34.9). The increased risk of bleeding complications was not observed when thienopyridine was discontinued (OR:2.52, 95%CI:0.83–7.70); however, it became apparent when it was continued perioperatively (OR:4.35, 95%CI:1.14–16.61).

CONCLUSIONS

This study reveals that thienopyridine increases the incidence of bleeding complications, particularly low-grade bleeding complications, following robot-assisted radical prostatectomy. These bleeding effects emerged when thienopyridine was continued perioperatively.

COI disclosure information
I have no financial relationships to disclosure.

Flow diagram of the study.

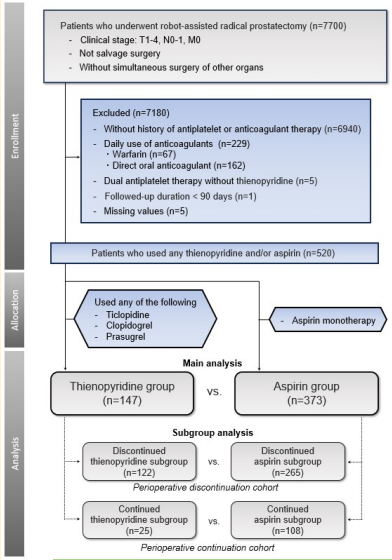

Patient background ① (Table1).

Table 1 Details of administrated antiplateles of the thienopyridine and aspirin group.

Parameter	Overall	Thienopyridine group	Aspirin group
Patients, no.	**520**	**147**	**373**
Administered antiplatelets, n (%)			
Thienopyridine	147 (28)	147 (100)	-
Ticlopidine	11 (2)	11 (7)	-
Clopidogrel	126 (24)	126 (86)	-
25mg	28 (5)	28 (19)	-
50mg	14 (3)	14 (10)	-
75mg	84 (16)	84 (57)	-
Prasugrel	10 (2)	10 (7)	-
Aspirin	422 (81)	49 (33)	373 (100)
100mg	410 (79)	47 (32)	363 (97)
200mg, or more	12 (2)	2 (1)	10 (3)
Cilostazol 100mg	3 (0.6)	3 (2)	-
DAPT	52 (10)	52 (35)	-
History, n (%)			
Coronary artery disease	231 (44)	65 (44)	166 (45)
Cerebral infarction	118 (23)	44 (30)	74 (20)
Carotid stenosis	41 (8)	15 (10)	26 (7)
Arhythmia	22 (4)	4 (3)	18 (5)
Cardiac valve surgery	4 (0.8)	1 (0.7)	3 (0.8)
Primary prevention	23 (4)	2 (1)	21 (6)
Others	111 (21)	20 (14)	91 (24)

DAPT, Dual antiplatelet therapy

Patient background ② (Table2).

Table 2 Patient characteristics before and after IPTW compared between the thienopyridine group and aspirin group.

Parameter	Total	*Unweighted study cohort* Thienopyridine group	vs. Aspirin group	SD (%)	*Weighted study cohort* Thienopyridine group	vs. Aspirin group	SD(%)
Patients, no.	**520**	**147**	**373**				
Median age, years (IQR)	71 (68-74)	71 (67-74)	71 (68-74)	-0.014	71 (67-75)	71 (68-74)	-0.023
ASA PS 3, or more, n (%)	99 (19)	39 (27)	60 (16)	0.257	20%	19%	0.013
BMI ≧ 25 kg/m2, n (%)	204 (39)	50 (34)	154 (41)	-0.151	38%	39%	-0.015
KDIGO CKD grade (eGFR), n (%)							
Grade 1, or 2 (60 mL/min/1.73 m^2, or n	333 (64)	89 (61)	244 (65)	0.101	65%	64%	-0.020
Grade 3a, or 3b (30–59 mL/min/1.73 m	172 (33)	51 (35)	121 (32)		32%	33%	
Grade 4, or 5 (29 mL/min/1.73 m^2, or k	15 (2.9)	7 (4.7)	8 (2.1)		3.4%	3.1%	
NCCN high risk group, or more, n (%)	248 (48)	74 (50)	174 (47)	0.074	48%	48%	0.002
Extended lymph node dissection, n (%)	107 (21)	25 (17)	82 (22)	-0.126	19%	20%	-0.040
Neurovascular bundle preservation, n (%	154 (30)	46 (31)	108 (29)	0.051	29%	29%	0.040
Preoperative hormonal therapy, n (%)	132 (25)	32 (22)	100 (27)	-0.118	27%	26%	0.024
Perioperative continuition of antiplatelets	133 (26)	25 (17)	108 (29)	-0.287	24%	26%	-0.036

Main analysis (Table3).

Table 3 Unweighted and weighted regression models which analyzed associations between the study outcomes and the group of the thienopyridine group compared on the aspirin group.

	Thienopyridine vs. Aspirin group					
Parameters	*Unweighted analysis*			*IPTW analysis*		
Binary outcomes	**Odds ratio**	**95% C.I.**	**P-value**	**Odds ratio**	**95% C.I.**	**P-value**
Bleeding complications	3.13	0.94-10.43	0.063	3.62	1.54-8.49	0.003
Low grade (C-D grade II, or less)	3.24	0.86-12.27	0.082	3.20	1.23-8.30	0.017
High grade (C-D grade III, or more)	2.55	0.16-41.01	0.51	5.23	0.78-34.90	0.088
Transfusion	3.86	0.64-23.37	0.14	6.35	1.75-23.01	0.005
Hemorrhagic shock	2.55	0.16-41.01	0.51	5.23	0.78-34.90	0.088
Thrombotic complication	0.68	0.070-5.70	0.68	0.27	0.048-1.499	0.13
Overall high-grade complications	1.50	0.58-3.90	0.40	1.31	0.70-2.45	0.40
Readmission	2.60	0.83-8.20	0.10	2.96	1.34-6.54	0.007
Continuous outcomes	**Estimate**	**95% C.I.**	**P-value**	**Estimate**	**95% C.I.**	**P-value**
Operation time, min	0.33	-7.60 to 8.26	0.93	-2.30	-9.57 to 4.97	0.53
Estimated blood loss, mL	3.04	-19.13 to 25.22	0.79	-9.26	-32.50 to 13.99	0.43
Hemoglobin deficit, median, mg/dL	0.001	-0.10 to 0.11	0.98	-0.004	-0.097 to 0.089	0.94

- Thienopyridine therapy was associated with a higher risk of bleeding complications , transfusion , and readmission.
- The increased risks of the thienopyridine group were detected for low-grade bleeding complications, but not for high-grade bleeding complications.

Subgroup analysis (Table4).

Table 4 Subgroup analyses: IPTW-regression models which analyzed associations between the outcomes and the group of the thienopyridine group compared on the aspirin group, in the cohorts of perioperative discontinuation (left) and continuation (right) of antiplatelets.

	Thienopyridine vs. Aspirin subgroup					
Parameters	*Perioperative discontinuation cohort*			*Perioperative continuation cohort*		
Binary outcomes	**Odds ratio**	**95% C.I.**	**P-value**	**Odds ratio**	**95% C.I.**	**P-value**
Bleeding complications	2.52	0.83 - 7.70	0.10	4.35	1.14 - 16.61	0.031
Low grade (C-D grade II, or less)	2.52	0.83 - 7.70	0.10	4.45	0.68 - 29.19	0.12
High grade (C-D grade III, or more)	NA	NA	NA	3.97	0.61 - 25.85	0.15
Transfusion	2.42	0.35 - 17.00	0.37	8.66	1.48 - 50.73	0.017
Hemorrhagic shock	NA	NA	NA	3.97	0.61- 25.85	0.15
Thrombotic complication	0.42	0.064 - 2.70	0.36	NA	NA	NA
Readmission	2.31	0.89 - 6.02	0.087	5.04	1.18 - 21.47	0.029
Continuous outcomes	**Estimate**	**95% C.I.**	**P-value**	**Estimate**	**95% C.I.**	**P-value**
Operation time, min	-3.80	-12.09 to 4.48	0.37	-1.53	-16.07 to 13.02	0.84
Estimated blood loss, mL	-8.15	-30.08 to 13.76	0.46	-13.44	-75.20 to 48.32	0.67
Hemoglobin deficit, median, mg/dL	-0.020	-0.13 to 0.087	0.72	0.020	-0.16 to 0.20	0.83

- The increased risk of bleeding complications was not observed when thienopyridine was discontinued.
- However, it became apparent when it was continued perioperatively.

3

Preventive measures for port-site hernia in Robotic Assisted Radical Prostatectomy

Ryoma Kurahashi, Hidekazu Nishizawa, Toshiki Anami, Takanobu Motoshima, Yoji Murakami, Junji Yatsuda, Tomomi Kamba
Department of Urology, Faculty of Life Sciences, Kumamoto University, Kumamoto, Japan

Kumamoto University

Background

With the spread of SARS-Cov-2 infection, the risk of infection due to pneumoperitoneum gas exposure during laparoscopic surgery has been pointed out. In our facility, robot-assisted urologic surgery is performed with a constant smoke evacuation pneumoperitoneum device (AirSeal®) to manage the gas exchange in a closed circuit. On the other hand, 12mm AirSeal® port site tend to be larger than other ports, and port site hernias often become a problem.

port site hernia case1

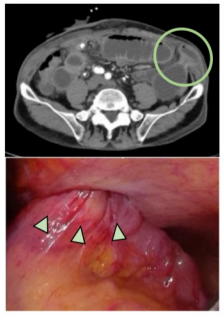

port site hernia case2

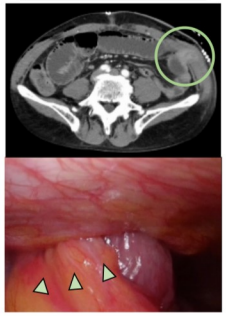

Port placement in our facility

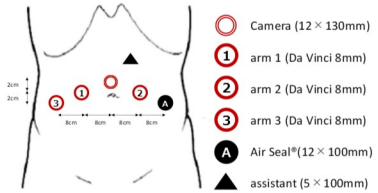

Due to the occurrence of port-site hernia to the 12mm AirSeal® port, we decided to perform a port suture from the abdominal cavity before the end of insufflation to ensure closure of the peritoneum.

Methods

Procedure of port suture

After vesicourethral anastomosis and drain placement

Needle delivery. (through AirSeal®)

Remove the AirSeal® temporarily, suture the peritoneum at the port.

Cut the suture. (through 5mm assistant port)

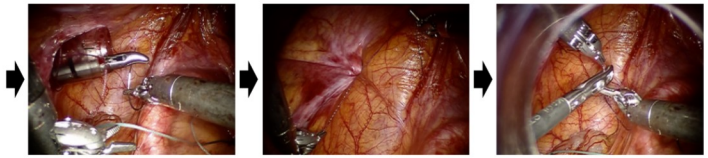

Reinsert AirSeal® and remove the needle.

Ligate the suture.

Cut and remove the excess suture. (through 5mm assistant port)

Results

Although this procedure is rather complicated, it can be performed in about 6 minutes on average, regardless of the patient's size or the surgeon's experience. None of the 89 patients who underwent the procedure developed port-site hernias.

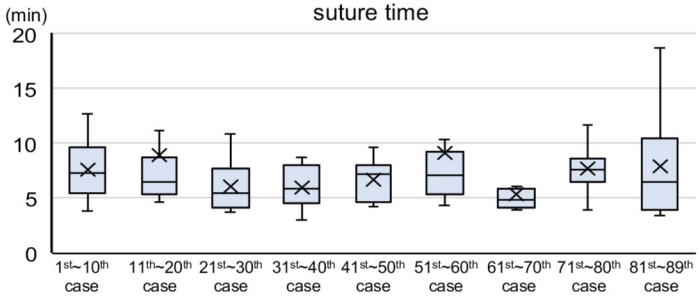

Discussion

Port-site hernias are especially noted to occur in ports larger than 10 mm. In early postoperative hernias, the peritoneum, anterior rectus sheath and posterior rectus sheath are often ruptured. It is more likely to occur if the peritoneum is not sutured.

Source	Study	Follow-up	Original Surgery, No. of Patients	No. of Cases of TSH	Incidence, %	Delay After Laparoscopy, Mean (Range)	Main Clinical Manifestation, No. of Cases	Hernia Site	Trocar Size in TSH, mm	Fascia in TSH Site Closed or Left Open, No. of Cases
Azurin et al.[1] 1995	Retrospective	1 Postoperative 1 surgeon visit	Cholecystectomy. 1300	10	0.77	8 mo (5-d-2 y)	Hernia without SBO. 6; Richter hernia, 1	Umbilical. all	10	Closed, all
Mayol et al.[2] 1997	Prospective	database Range, 3-51 mo	Cholecystectomy. 373; fundoplication, 8; colon surgery, 9; other abdominal operations, 13	6	1.53	Not written	Hernia without SBO: all	Umbilical. all	10	Closed 5, left open, 1
Nassar et al[3]	Prospective	Second appointment; 2-6 mo	Cholecystectomy. 870	16	1.8	6 mo (2-16 mo)	Hernia without SBO. 15; SBO. 1	Umbilical. 15; right side, 1	10; right side, 5	Closed, 1
Sanz-Lopez et al.[4] 1999	Retrospective	Mean, 3 y; range, 1-5 y	Cholecystectomy. 123	2	1.6	14 mo; (10-18 mo)	Hernia without SBO. all	Umbilical, 1; umbilical and xiphoid, 1	10	Closed, 2; left open, 1
Coda et al.[14] 2000	Retrospective	Not written	Laparoscopic surgery, 1287 (94% biliary tract)	13	1.0	8.8 mo; (3-36 mo; except protrusion, 1)	Hernia without SBO. 11; strangulation, 1; protrusion of omentum, 1	Umbilical. 12; right side, 1	11-12	Closed, all
Bowrey et al.[5] 2001	Retrospective	Mean, 12 mo; range, 6 wk-61 mo	Fundoplication. 320	9	2.8	(4-21 mo)	Hernia without SBO. all	Umbilical. all	10	Closed, all
Susmallian et al.[6] 2002	Retrospective	Not written	Gastric banding. 459	3	0.65	3 wk-4 mo (6 mo)	Hernia without SBO. all	Left upper	11	Left open, all

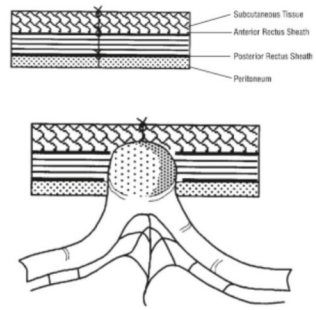

Tonouchi H, et al., Trocar Site Hernia. Arch Surg. 2004;139(11):1248-1256.

In pelvic robotic-assisted surgery, port-site hernias are more likely to occur at the lateral side ports that are in close proximity to the intestinal tract and coincide with the Spigelian hernia belt.

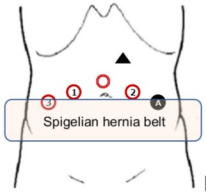

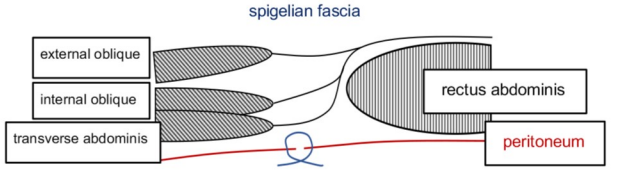

Peritoneal suture can reinforce spigelian fascia and prevents hernias.

Conclusions

Secure suturing from the abdominal cavity may prevent the development of hernias. By standardizing the procedure, suture operations can be performed in a relatively short time without being affected by operating skill or patient body shape. Fascial closure should be aggressively considered for port wounds greater than 10 mm below the arch line.

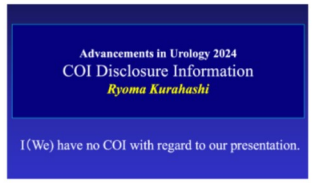

4

Differences in incidence and clinicopathologic features of secondary bladder cancer after long-term follow-up of brachytherapy and radical prostatectomy for localized prostate cancer.

Kotaro Obayashi [1], Go Kimura [1], Hayato Takeda [1], Jun Akatsuka [1], Yuki Endo [1], Yuka Toyama [1], Hiroyuki Muramatsu [2]
Katsuya Maebayashi [2], Shinichiro Kumita [2], Yukihiro Kondo [1]

1) Department of Urology, Nippon Medical School Hospital, Tokyo, Japan
2) Division of Radiation Oncology, Nippon Medical School Hospital, Tokyo, Japan

BACKGROUNDS

Although there studies have been reported that brachytherapy (BT) for prostate cancer is associated with an increased incidence of metachronous urinary bladder cancer (MBC), few studies have clarified differences in the clinicopathological features (CPF) of MBC between BT and prostatectomy (RP). We studied the risk and clinicopathological CPF of MBC between RP and BT groups in our hospital after long-term follow-up.

METHODS

We reviewed 504 patients treated with BT and 471 patients treated with RP between 2006 and 2017 in our hospital. We compared the incidence of MBC and the CPF including the tumor number, location within the urinary bladder, histology, and time from BT or RP to the MBC occurrence between BT and RP. The differences between the two groups were analyzed using the Mann-Whitney U and chi-square tests. Furthermore, in the BT group, the radiation dose distribution within urinary bladder was estimated and whether they met the criteria of radiation-induced malignancies was judged adopting the criteria as described in table 1 proposed by Sakai et al in1981; different pathological feature from the organ of origin, the follow-up duration after radiation therapy (over 5 years), and whether the lesion is located in the irradiated field (A1 reliability in table 1).

RESULTS

After a median follow-up time of 107 months (13-209), a total of 11 cases of MBC occurred in the BT group (2.2%) and 7 in the RP group (1.5%). Histologically, all MBC cases were urothelial carcinomas (UC). The median time from initial treatments to the occurrences of MBC was 65 months (12-121) in BT and 100 months (4-126) in RP (p=0.469). Average tumor number was not different between the groups (BT:1.4, RP:1.9, p=0.589).

The incidence of MBC in each location within the bladder for BT vs. RP was 9 vs 1 in lateral wall, 1 vs 4 in the posterior wall, 0 vs 2 in the dome, and 1 vs 0 in the trigone. The incidence in the lateral wall was significantly higher in BT than in RP (p=0.001). There were 3 muscle-invasive cases in BT and 1 case in RP (p=1.00). High-grade urothelial carcinoma occurred significantly more in BT 10 patients than in RP 1 patient(p=0.001).

The details are shown in figure and table 3.

CONCLUSIONS

Long-term follow-up showed that the risk of MBC after BT was similar to that after RP. MBC after BT occurred significantly more frequently in the lateral wall and had a higher grade carcinoma compared to those after RP.

RESULTS

【Figure】 【The location of MBC within the bladder after RP】

GS: Gleason Score PSA: Prostate Specific Antigen

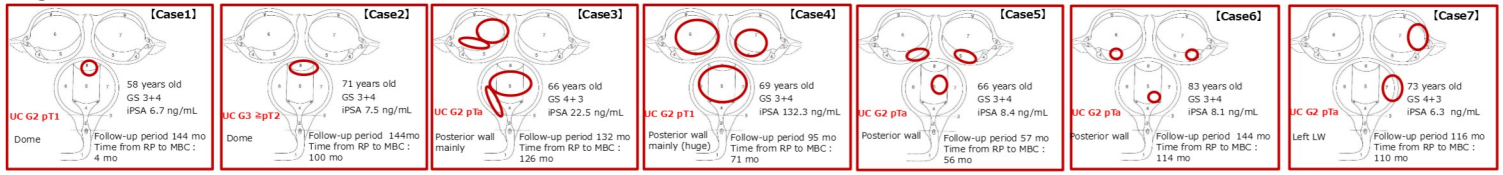

【The location of MBC within the bladder after BT】

LW: Lateral Wall

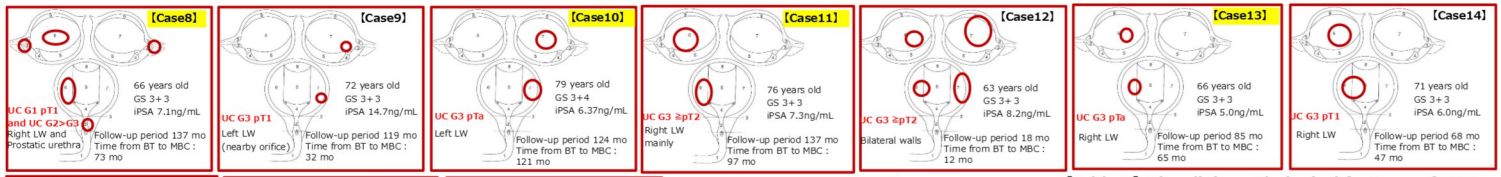

Red circles mean the locations and sizes of MBC.

Six MBC were judged as radiation-induced (yellow shadow).

The estimated max and mean radiation doses to the lateral walls within urinary bladder were showed in table 2.

【Table 1】 Sakai's criteria

Reliability		Criteria			
		Histological type	Organ of origin	Latent period	Site of origin
A (High)	1	different	different		
	2	different	same		
B (Medium)	1	same	different (non-continuous)	more than 5 years*	within the irradiated site
	2	same	different (continuous)		
C (Low)	1	same	different (non-continuous)		
	2	same	different (continuous)		

*This criteria is excluded when leukemia developed as a second malignancy.

【Table 2】 Radiation doses of MBC cases after BT

Case No.	Right LW Max (Gy)	Right LW Mean (Gy)	Left LW Max (Gy)	Left LW Mean (Gy)
8	27.92	10	33.71	10.43
9	64.77	10.47	27.46	7.81
10	68.47	11.6	98.93	13.46
11	17.55	5.52	40.29	7.24
12	76.81	20	118.88	26
13	31.14	7.69	56.38	11.42
14	136.81	29.46	40.99	11.21
15	22.71	9.81	46.07	12.98
16	177.56	35.83	45.82	19.5
17	52.96	16.24	50.35	10.2
18	27.92	10	33.71	10.43

【Table 3】 The clinicopathological features of MBC

	BT (n=504)	RP (n=471)	p-value
≧pT2	3 (0.6%)	1 (0.21%)	1.00
≦pT1	8 (1.59%)	6 (1.27%)	1.00
G3	10 (1.98%)	1 (0.21%)	0.001
G1-2	1 (0.2%)	6 (1.27%)	0.001
The median time to MBC (mo)	65	100	0.469
Lateral wall	9 (1.79%)	1 (0.21%)	0.001
Right wall	5 (0.99%)	0	0.001
Left wall	4 (0.79%)	1 (0.21%)	0.001
Posterior wall	1 (0.2%)	4 (0.67%)	0.006
Dome	0	2 (0.42%)	0.002
Trigone	1 (0.2%)	0	0.083
Average tumor number	1.4	1.9	0.589

Advancements in Urology 2024 Disclosure of Conflict of Interest

We have no COI with regard to our presentation.

5

The efficacy of androgen receptor signaling inhibitor therapies for metastatic hormone-sensitive prostate cancer at Yamaguchi University

Takanori Tokunaga, Nakanori Fuji, Keita Kobayashi, Hideaki Ito, Hiroshi Hirata, Koji Shiraishi
Department of Urology, Graduate School of Medicine, Yamaguchi University

Objective

Androgen receptor signaling inhibitor (ARSI) for metastatic hormone-sensitive prostate cancer (mHSPC) is available since the approval of abiraterone in 2018.
We report the efficacy with ARSI for mHSPC at our hospital.

Material and Methods

Study design

This study was retrospective study and approved by the Ethical Review Committee of Yamaguchi University (ID 2023-042). This study included patients who treated with ARSI for mHSPC between February 2018 to March 2023 at Yamaguchi University Hospital.

Adverse Events

Adverse events were evaluated according to the Common Terminology Criteria for Adverse Events, version 5.0.

Statistical analysis

The Kaplan–Meier method was used to estimate time to CRPC. Log-rank tests were used for intertreatment comparisons. The predictors of time to CRPC were extracted using univariate and multivariate logistic regression analyses. Statistical analyses were performed using JMP pro version 15.0 (SAS Cary, NC, USA). The two-sided significance level of the tests was 5%, and the confidence interval estimation was 0.95.

Results

Table 1. Patient and tumor characteristics (n=41)

Age, y median (range)		73 (62-89)	**Site of metastasis (%)**		
	0	30 (73%)	Extrapelvic Lymph nodes		16 (39%)
ECOG PS	1	5(12%)	Visceral		5 (12%)
	≥2	6 (15%)	Bone		34 (83%)
BMI, kg/m² median (range)		22.01 (16.2-31.9)	**Number of bone metastases, n**		
Symptoms at first visit	No	12 (29%)		1	13 (32%)
	Yes	29 (71%)	EOD score	2	10 (24%)
Initial PSA, ng/ml median（range)		315（4.27-5401）		≥3	11 (27%)
	4+3	2 (5%)	**BSI, median (range)**		0.84 (0-11.12)
	4+4	12 (29%)	**Volume**	low	15 (37%)
Gleason score	4+5	15 (36%)		high	26 (63%)
	5+4	4 (10%)	**Risk** *LATITUDE Clinical Trials	low	10 (24%)
	5+5	8 (20%)		high	31 (76%)

Abbreviations: ECOG PS, Eastern Cooperative Oncology Group Performance Status; BMI, Body Mass Index; EOD, extent of disease
BSI, bone scan index as measured by BONENAVI®
※EODI: 1－5 lesions, II: 6－20 lesions, III: more than 20 but less than EOD IV, IV: generalized uptake, super scan or more than 75% of axial skeleton.

Table 2. Univariate and multivariate analysis of predictive factors of time to CRPC

		Univariate			Multivariate		
Variable		HR	95% CI	p value	HR	95% CI	p value
Age	≥75 vs <75	1.20	0.21-6.60	0.833			
ECOG PS	≥1 vs 0	2.17	0.39-11.94	0.374			
BMI	>22.5 vs ≤22.5	0.80	0.23-8.61	0.691			
PSA	≥300 vs <300	2.03	0.37-11.13	0.411			
GS primary grade 5	No vs Yes	**14.72**	1.70-126.93	**0.0144**	**11.54**	1.27-104.49	**0.0295**
Symptoms at first visit	No vs Yes	0.84	0.15-4.59	0.837			
Site of metastasis							
Extrapelvic lymph nodes	No vs Yes	2.57	0.27-14.03	0.276			
Visceral	No vs Yes	3.54	0.63-19.66	0.148			
EOD	≥3 vs <3	**6.42**	1.05-39.27	**0.0441**	3.57	0.55-23.03	0.1807

Abbreviations: ECOG PS, Eastern Cooperative Oncology Group Performance Status; BMI, Body Mass Index; GS, Gleason Score
EOD, extent of disease
※EODI: 1－5 lesions, II: 6－20 lesions, III: more than 20 but less than EOD IV, IV: generalized uptake, super scan or more than 75% of axial skeleton.
HR; Hazard ratio, CI; Confidence intervals

Table 3. Adverse events in patients who received ARSI (n=41)

	Grade1	Grade2	Grade3	Grade4
AST/ALT increased	1 (2.4%)	1 (2.4%)	1 (2.4%)	—
hyperglycemia	—	4 (9.8%)	—	—
Rash	—	5 (12.2%)	3 (7.3%)	—

AST; aspartate aminotransferase ALT; alanine aminotransferase

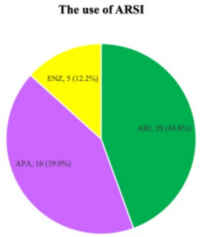

Figure. Kaplan–Meier projection of time to CRPC

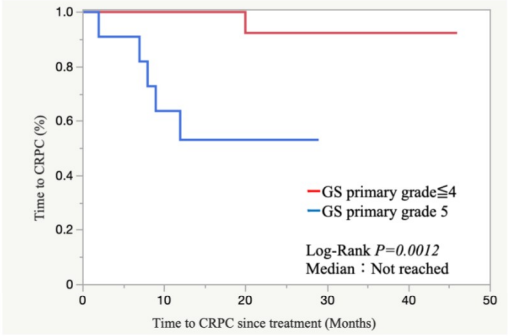

CRPC, castration-resistant prostate cancer

Discussion and Conclusion

- ARSI for mHSPC showed preferable response without life-threatening adverse effect.
- Several studies suggested that patients treated with ARSI for mHSPC who had high GS, high disease burden, baseline pain or opioid use and baseline unfavorable laboratory values (high LDH and ALP, low Hb) had worse outcomes.
- Further intensified treatments such as triplet therapy may be considered in patients in Gleason score primary grade 5.

Advancements in Urology 2024
COI Disclosure Information
Takanori Tokunaga, Nakanori Fuji, Keita Kobayashi, Hideaki Ito, Hiroshi Hirata, Koji Shiraishi

I（We) have no COI with regard to our presentation.

6

Baseline Tumor Size as a Prognostic factor for Immune Checkpoint Inhibitor Treatment in Metastatic Urothelial Carcinoma Refractory to First-Line Platinum Combined Chemotherapy

Yuki Endo , Jun Akatsuka, Hayato Takeda, Kotaro Obayashi, Masato Yanagi, Yuka Toyama, Hikaru Mikami, Hiroya Hasegawa, Mikio Shibasaki, Ryota Funato, Shogo Miyauchi, Mami Taniuchi, Honami Kishi, Go Kimura, Yukihiro Kondo, Nippon Medical School Hospital, Department of Urology, Tokyo, Japan

BACKGROUND

- Baseline tumor size (BTS) is a critical prognostic factor in melanoma and NSCLC for patients (Pts) under immune checkpoint inhibitor (ICI) therapy, with larger BTS linked to poorer outcomes.
- However, literature on the relationship between BTS and prognosis in metastatic urothelial carcinoma (mUC) is notably absent.
- This underscores the need for research into BTS's role in mUC Pts prognosis, especially for those undergoing ICI treatment.

MATERIAL & METHODS

- 56 Pts with platinum-refractory mUC (PRmUC) who received pembrolizumab (PB) between 2018-2022 at NMS.
- OS rates were assessed using Kaplan-Meier curves. The Objective Response Rate (ORR) was determined based on RECIST (ver. 1.1) criteria.
- BTS was evaluated using CT scan taken within 1 month(M) before ICI therapy, following RECIST criteria.
- BTS was estimated using the maximum BTS (mBTS) and total BTS (the sum of target lesions). Pts were categorized into 2 groups based on the cut-off values calculated using the Area Under Curve (AUC) method: tBTS (≦50mm vs >50mm) and mBTS (≦30mm vs >31mm).

RESULT

- 56 Pts, with a median follow-up of 17.4 Ms. (Table1)
- The median OS was 23.4 Ms, and the 1-year OS rate was 33% and the ORR was 25%. (Table1)
- PFS was shorter in Pts with large tBTS (p=0.015) (Fig.1-a) and large mBTS (p=0.002) (Fig.1-b). While OS was significantly shorter in Pts with large mBTS (p=0.019)(Fig1-d), OS with large tBTS did not show significance.(Fig1-c)

Table 1. Patients background

Patient background			
		n	(%)
sex			
	female	15	26.8%
	male	41	73.2%
		median(range)	
age		74 (31 - 86)	
follow up months		17.4 (6.2 - 72.3)	
		n	(%)
primary location			
	UTUC	28	(50.0%)
	LTUC	28	(50.0%)
pathological subtype (variant)			
	yes	29	(51.8%)
	no	27	(48.2%)
number of GC courses			
	1	12	(21.4%)
	2	26	(46.4%)
	3	18	(32.1%)
metastatic locations			
	Lymph node	33	(58.9%)
	Lung	21	(37.5%)
	Liver	7	(12.5%)
	Peritonium	1	(1.8%)
	Bone	7	(12.5%)
	Local	17	(30.4%)
best response			
	CR	3	5.4%
	PR	11	19.6%
	SD	18	32.1%
	PD	24	42.9%
		median(range)	
total baseline tumor size(mm)		56 (5 - 250)	
maximum baseline tumor size (mm)		20 (0 - 98)	

Fig 1. PFS and OS in each group

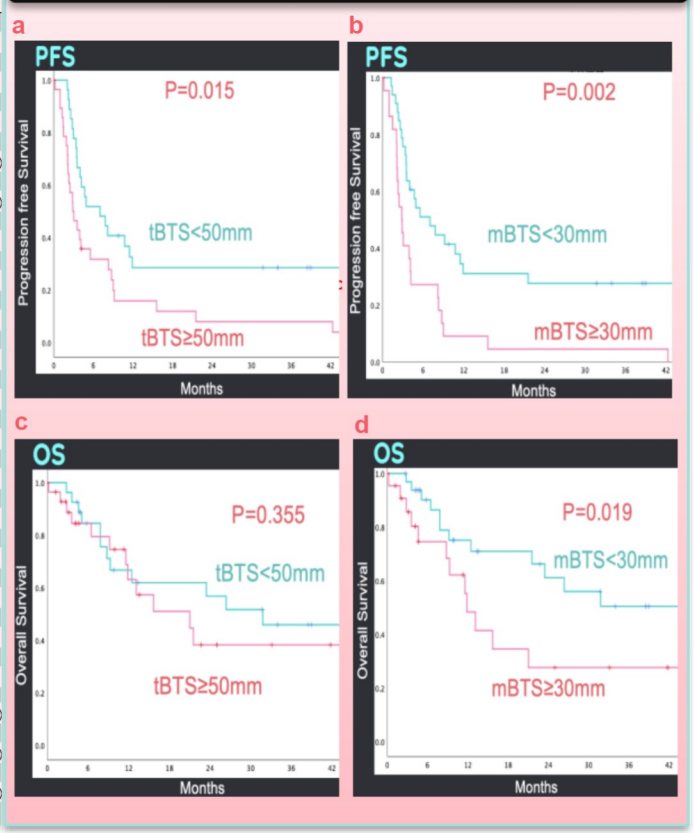

Conclusions

- Larger mBTS was associated with shorter PFS and OS.
- No OS difference was seen with larger tBTS, probably due to subsequent Enfortumab vedotin therapy.
- ICI treatment should be administered earlier before tBTS of ≤50 and mBTS of≤30 in Pts with PRmUC.
- Cases with tumor size around cutoff values may also consider debulking surgery to improve outcomes.

COI

NONE

7

A single-institution experience of intra-arterial chemoradiation therapy for non-metastatic bladder cancer

○Fumiakira Yano, Ryosuke Suda, Masaki Matsuda, Takanori Mochizuki, Satoru Kira, Takuji Araki, Hiroshi Onishi, Takahiko Mitsui

University of Yamanashi Hospital

INTRODUCTION

Total cystectomy is a standard treatment method for locally invasive bladder cancer or high-risk non-muscle-invasive bladder cancer who develop disease recurrence following BCG therapy. However, this approach can be intolerable or decrease quality of life, especially for the elderly. A trimodality therapy approach that combines radical transurethral resection of the bladder tumor (TURBT), chemotherapy, and radiation therapy has since long been applied as an alternative approach for patients who require cystectomy. (1-2)

We report our results of trimodality therapy consisting of TURBT, external beam radiation therapy (EBRT), and Intra-arterial chemotherapy (IACT) for patients with non-metastatic bladder cancer.

PATIENTS AND METHODS

We retrospectively reviwed18 patients who underwent trimodality therapy at our hospital between 2016 and 2023. This treatment was performed in patients who were unable to undergo radical cystectomy and urinary diversion due to such conditions as advanced age, severe co-morbidity, and refusal to undergo surgery. We used radiotherapy to the bladder at 60-66 Gy/30-33 fr and cisplatin 25-100 mg/body administered twice or three times at 3-week intervals through the bilateral bladder arteries. The patients were followed up with clinical and radiographic investigations and bladder biopsy was performed as needed. Toxicity was graded according to CTCAE ver 5.0.

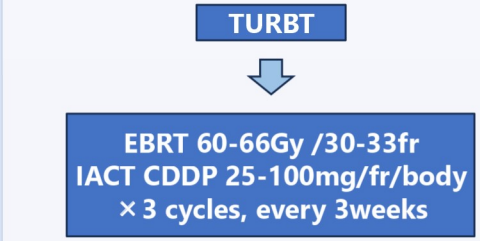

Figure 1. Treatment protocol

RESULTS

Table 1. Patient Characteristics (N = 18)

Age, median years(range)	80(46-87)
Gender, n (%)	
Male	11(61.1)
Female	7(38.9)
ECOG PS, n (%)	
0-1	18(100)
≧2	0(0)
T stage, n (%)	
Ta	2(11.1)
T2	11(61.1)
T3	4(22.2)
T4	1(5.6)
Follow up period, month(range)	20(2-69)

Abbreviations: ECOG PS, Eastern Cooperative Oncology Group performance status.

- Two patients with stage Ta had early recurrence after BCG treatment.

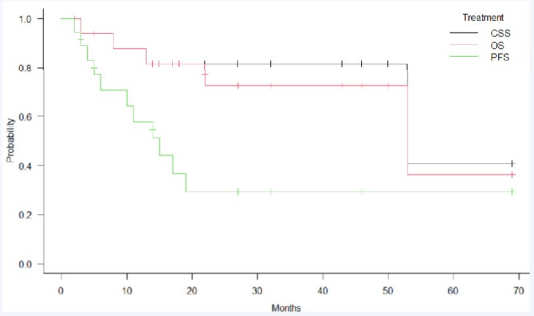

Figure 2. OS, CSS, PFS curve of all patients.

- 3-year Overall survival (OS) rate was 70.0%, cancer-specific survival (CSS) rate was 81.6% and progression-free survival (PFS) rate was 28.6%, respectively.

N of patients (%)	All grades	Grade ≧3
Cystitis	18(100)	0(0)
Enteritis	4(22.2)	0(0)
Dermatitis	6(33.3)	0(0)
Blood toxicity		
Anemia	1(5.6)	0(0)
Neutropenia	2(11.1)	1(5.6)
Thrombocytopenia	2(11.1)	0(0)

Table 2. All adverse event related to treat

- Adverse events included enteritis, dermatitis, cystitis, leukopenia, anemia, and thrombocytopenia; except for one case with grade 3 neutropenia, all others were grade 2 or less.

CONCLUSIONS

Intra-arterial chemoradiotherapy for bladder cancer is well tolerated and may be a viable option for patients who refuse radical cystectomy.

REFERENCES

1. Mori K, et al, Long-term follow up of patients with invasive bladder carcinoma receiving combined cisplatin-based intra-arterial chemotherapy and radiotherapy. Int J Urol 14: 591-594, 2007.
2. Yoshioka H, et al, Treatment Results of Radiotherapy Combined with Balloon-occluded Arterial Infusion Chemotherapy for Invasive Bladder Cancer. Anticancer Research February 2016, 36 (2) 731-736;
3. National Cancer Institute. Common terminology criteria for adverse events v5.0(CTCAE). https://ctep.cancer.gov/protocoldevelopment/electronic_applications/docs/ctcae_v5_quick_reference_5x7.pdf (accessed November 27 2017)

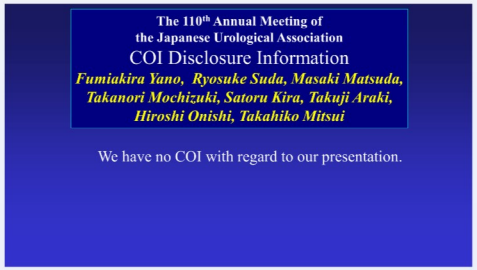

8

Establishment of muscle-invasive bladder cancer models by molecular subtype

Department of Urology, Kyoto University Graduate School of Medicine, Kyoto, Japan[1] , Lineberger Comprehensive Cancer Center, University of North Carolina at Chapel Hill[2]
Hideaki Takada[1] Akihiro Hamada[1,2] Yuki Kita[1] Ryoichi Saito[1] Kaoru Murakami[1] Kenji Nakamura[1] Ryosuke Ikeuchi[1] Syuhei Koike[1] Takashi Kobayashi[1]

【Methods】 Recently, molecular subtype classification of muscle-invasive bladder cancer based on gene expression profiles has attracted attention, and currently six subtypes have been proposed, with differences in response rates to chemotherapy and IO (immuno-oncology) treatment reported among the subtypes. Individualized therapeutic selection based on molecular subtypes is considered necessary, but due to the lack of preclinical models, little progress has been made in studying individual treatment strategies. To address this clinical challenge, we are working to establish disease models based on a molecular biological understanding the diversity of bladder cancer.

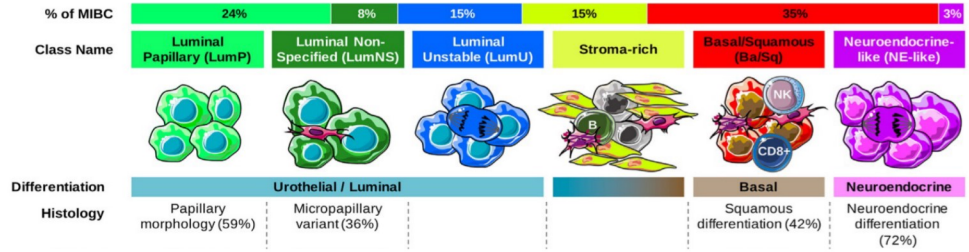

Kamoun et al. Eur Urol. 2020 Apr;77(4)

【Results】 We focused on organoids, a three-dimensional tissue culture system, as a new model for bladder cancer carcinogenesis. We removed the bladder of mice in which *Trp53* mutation and expression of Cas9-GFP were induced specifically in Krt5-positive cells, which are considered to be one of the origin cells of bladder cancer. GFP-positive cells isolated from the urothelial cells were grown in 3D culture with Matrigel, resulting in the successful establishment of organoids (K5-mUrorganoid; *Trp53*$^{R172H/+}$). Furthermore, we generated *Pten*-KO organoids (K5-mUrorganoid: *Trp53*$^{R172H/+}$; *Pten*$^{-/-}$) by infection with adeno-associated virus (AAV). These cells were transplanted subcutaneously into nude mice and formed tumors that histologically resembled human basal-squamous type with squamous differentiation, and were also found to be viable in immunocompetent mice.

Fig.1 Overview of experimental system

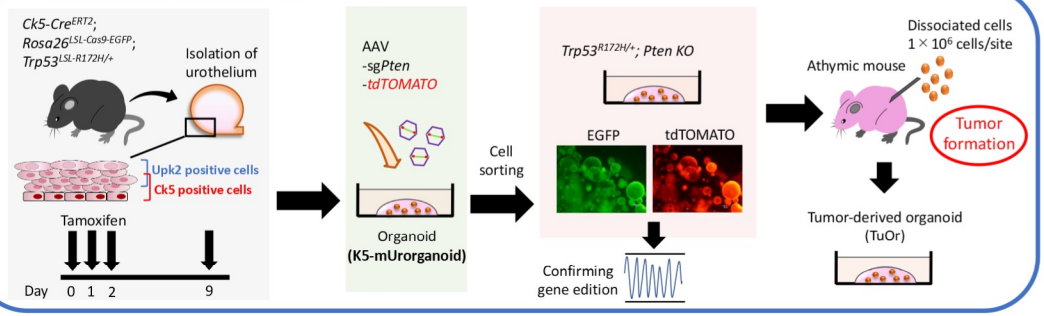

Fig.2 *Trp53*$^{R172H/+}$;*Pten*$^{-/-}$ K5-mUrorganoid formed tumors when transplanted into athymic mice

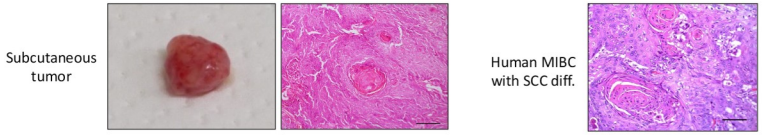

✓ Histologically similar to Basal/Squamous subtype of human MIBC

Fig.3 Loss of wild-type Trp53 allele and Pten loss confer in vivo tumorigenic ability to K5-mUrorganoid in athymic mice

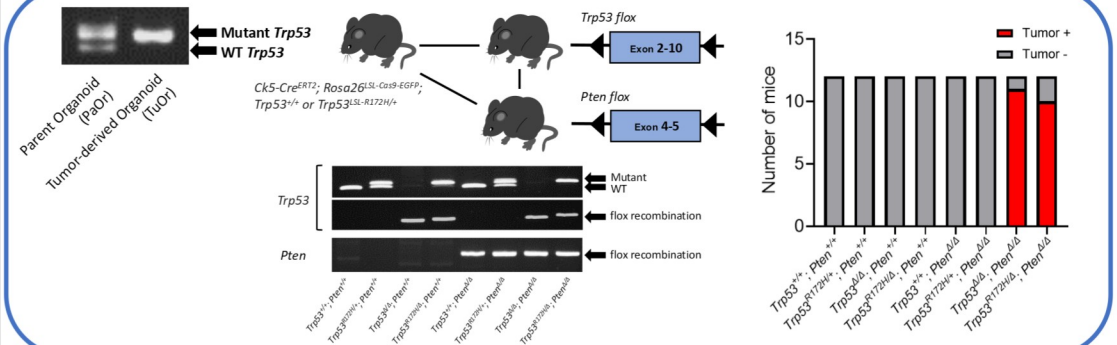

Fig.4 Tumors harbor molecular characteristics of the Basal/Squamous subtype of human MIBC

Modified from Masuda et al. AM J Pathol. 2020;190(8)

Fig.5 *Trp53*$^{R172H/Δ}$;*Pten*$^{Δ/Δ}$ K5-mUrorganoid showed higher tumor formation rate in immunocompetent mice

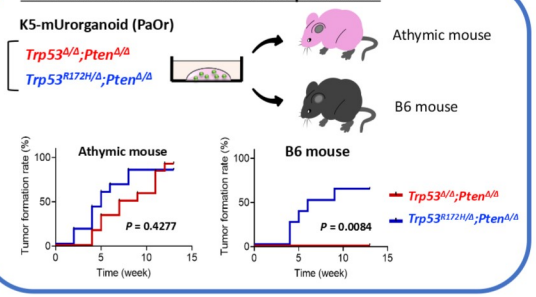

【Conclusions】 We have successfully established a mouse model of Basal/Squamous subtype bladder cancer. We are currently investigating factors involved in treatment response and resistance to IO drugs by studying the response of this model. Further studies are needed to establish models for other bladder cancer subtypes.

Fig.6 "Future Plan" To establish novel mouse models by molecular subtypes

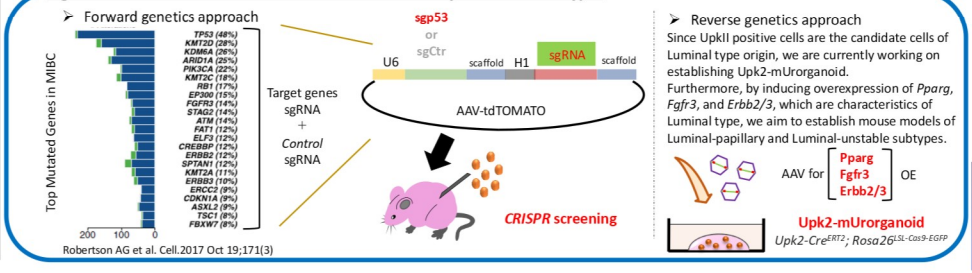

Clinicopathologic analysis of predictive factors for oncological and functional outcomes in minimally invasive treatment for cT1 renal cell carcinoma

Kensuke Bekku[1], Tomoaki Yamanoi[1], Mayu Uka[2], Noriyuki Umakoshi[2], Tatsushi Kawada[1], Takuya Sadahira[1], Satoshi Katayama[1], Takehiro Iwata[1], Shingo Nishimura[1], Kohei Edamura[1], Tomoko Kobayashi[1], Yasuyuki Kobayashi[1], Yusuke Matsui[3], Takao Hiraki[3], Motoo Araki[1]

1.Department of Urology, Okayama University Graduate School of Medicine, Dentistry, and Pharmaceutical Sciences, Okayama, Japan
2.Department of Radiology, Okayama University Hospital, Okayama, Japan
3.Department of Radiology, Okayama University Graduate School of Medicine, Dentistry, and Pharmaceutical Sciences, Okayama, Japan

9

Abstract

Introduction and objectives:
Tumor-associated factors including tumor complexity play an important role in determining appropriate treatment strategies for small renal cancers. This study aims to evaluate the impact of those on oncological and functional outcomes following minimally invasive treatments for small renal cancers.
Materials and methods:
435 patients with cT1 (<7cm) renal cell carcinoma (RCC) who underwent either robot-assisted partial nephrectomy (RAPN) or percutaneous cryoablation (PCA) divided into training and validation cohort at a ratio of 7:3. All patients were scored according to the modified R (radius, tumor size), E (endophytic properties), N (nearness to the collecting system or sinus), A (anterior or posterior), L (location to the polar line) nephrometry score (m-RENAL score). The primary endpoint was achieving a trifecta, comprising the absence of treatment failure and major complications, as well as preserving renal function. A nomogram was developed using tumor-associated factors and other clinicopathologic factors to predict trifecta achievement. The receiver operating curve (ROC) was utilized to validate the nomogram.
Results:
The trifecta was achieved in 157 (89%) out of 176 RAPN patients and 229 (88%) out of 259 PCA patients, respectively (P=0.8). For developing and validating the nomogram, a total of 305 and 130 patients were assigned to the training and validation cohorts respectively. Multivariate analysis indicated that the L domain of the m-RENAL score was the sole factor associated with trifecta achievement (P=0.009). The resulting nomogram predicting trifecta achievement included the type of intervention, R, E, N, and L domains of the m-RENAL score, histologic subtype, and pretreatment eGFR value. The area under the curve for the ROC was 0.72 for the training cohort and 0.56 for the validation cohort.
Conclusion:
The L domain of the m-RENAL score emerged as the solo independent predictor of trifecta achievement. The nomogram holds the potential to serve as a valuable tool for predicting outcomes for minimally invasive treated cT1 RCC.

Background

Ablation therapy for small renal cancer can achieve comparative outcomes with partial nephrectomy in terms of cancer control and preserving renal function while it is often recommended for selected patients deemed unfit for surgery.

Patients and methods

- A total of 435 patients with cT1 (<7cm) renal cancer who underwent RAPN or PCA between 2012 and 2021 at our institution
- Exclusion criteria
  - a history of renal cancer treatment
  - an inherited disease related to renal cancer
  - a history of renal replacement therapies
  - insufficient data
- Histology, preoperative renal function, and modified RENAL score[1)] (in which the R domain was adjusted to assign tumors a value of 1 if <3cm, 2 if 3-4cm, or 3 if >4cm) were collected and assessed
- All patients were divided into training and validation cohorts at a ratio of 7 : 3. A multivariable logistic regression model was applied to the training cohort to develop a nomogram

The requirements for Trifecta achievement[2)]

- absence of technical failure (no positive surgical margin for RAPN and no recurrence within 6 months for PCA)
- absence of major complications (CD grade 3 or more) in 3 months after the treatments
- absence of significant (≥25%) decline in eGFR from the baseline at 1 year after the treatments

Uni- and multivariable logistic regression analysis

	Univariable analysis Odds ratio (95% CI)	P-value	Multivariable analysis Odds ratio (95% CI)	P-value
Intervention(RAPN)	1.3 (0.6-2.7)	0.6	1.4 (0.6-3.3)	0.4
mR	0.6 (0.4-0.99)	0.045	0.7 (0.3-1.2)	0.2
E	1.2 (0.7-1.9)	0.5	1.2 (0.7-2.3)	0.5
N	0.6 (0.4-1.0)	0.07	0.7 (0.4-1.3)	0.3
L	0.5 (0.3-0.8)	0.03	0.5 (0.3-0.9)	0.009
Histology(non-clear)	1.1 (0.4-3.4)	0.8	1.0 (0.3-3.4)	0.9
eGFR ≥60	0.4 (0.2-0.9)	0.02	0.5 (0.2-1.0)	0.07
mRENAL score	0.7 (0.6-0.9)	0.005		

Nomogram

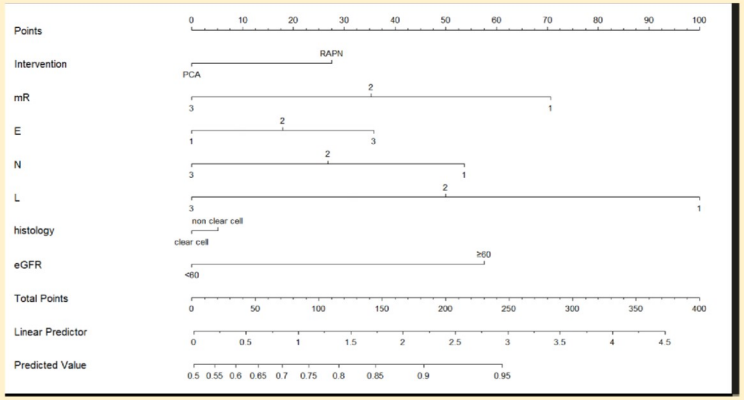

Sample cases

	Variables	Possibility of trifecta
1	mRENAL 1.1.3.3. eGFR <60 Clear-cell	RAPN 77% PCA 68%
2	mRENAL 1.2.1.1. eGFR ≥60 Clear-cell	RAPN >95% PCA >95%

ROC analysis

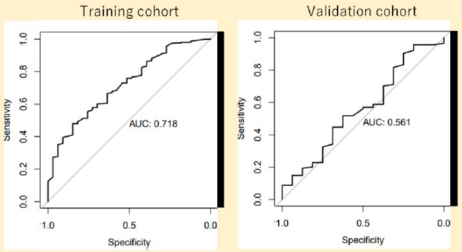

Conclusions

- Among tumor-associated factors, tumor location was solely associated with trifecta achievement on multivariable analysis.
- While the nomogram holds the potential to be a useful tool, further validation using a large cohort will be necessary.

References

1) Gaham et al. http://dx.doi.org/10.1016/j.urology.2014.08.026
2) Pandolfo et al. doi:10.1089/end.2022.0478

Advancements in Urology
An AUA/JUA Symposium 2024
COI Disclosure Information
Kensuke Bekku

We have no COI regarding our presentation

Comparative Effectiveness of TKI Monotherapy and ICI Combination in First-Line Advanced Renal Cell Carcinoma Treatment.

Wonseok Seo[1], Minekatsu Taga[1], Keisuke Ueki[1], Takao Nishikawa[1], Nodoka Okubo[1], Tadashi Kakitsuba[1], Yusuke Fukiage[1], Yoshinaga Okumura[1], Hisato Kobayashi[1], Manami Tsutsumiuchi[1], Masaya Seki[1], So Inamura[1], Masato Fukushima[1], Naoki Terada[1]

1) Departments of Urology, Faculty of Medical Sciences, University of Fukui

Advancements in Urology:
An AUA/JUA symposium (2024)
COI Disclosure Information
Wonseok Seo

I (We) have no COI with regard to our presentation.

Abstract

10

<Background>

Several drugs, such as TKIs and ICIs, have gained approval for treating advanced renal cell carcinoma (RCC). This study aimed to compare the efficacy between TKI monotherapy and ICI combined therapy as first-line treatments for advanced RCC.

<Methods>

This study included patients who received first-line medical treatment for advanced RCC between April 2007 and November 2023 at our hospital. The progression-free survival (PFS), overall response rate (ORR) and overall survival (OS) were evaluated and compared between TKI monotherapy group and ICI combined therapy group.

<Results>

In 79 patients (59 male and 20 female), median (range) age was 69 years (35-86), 44 had metachronous and 35 synchronous metastasis. The number of patients received TKI monotherapy and ICI combined therapy were 49 and 30, respectively. IMDC risk group distribution was favorable 16%, intermediate 62%, poor 21% (TKI group: 18% / 69% / 12%, ICI combined group: 13% / 50% / 37%). Median PFS was 7.4 months in TKI group and 10.8 months in ICI combined group (p=0.08). The ORR was 0.35 in TKI group and 0.63 in ICI combined group (p=0.02). Median OS was 42.9 months in TKI group, while it was not reached in ICI combined group (p=0.5).

<Conclusions>

ICI combined therapy had significantly higher response rate and tended to be longer time to progression than TKI monotherapy. Our retrospective study indicated that ICI combined therapy was more effective than TKI monotherapy as the first-line treatment for advanced RCC.

Background

The treatment landscape for advanced or inoperable renal cell carcinoma (RCC) has traditionally revolved around molecularly targeted therapies, in which tyrosine kinase inhibitors (TKIs) have played a pivotal role. However, the advent of immune checkpoint inhibitors (ICIs) has led to significant improvements in treatment efficacy[1]. The possibility of using not only dual immune checkpoint inhibitors, but also combination therapy with TKIs has broadened the spectrum of treatment options for advanced RCC. Therefore, we performed a retrospective comparative analysis between TKI monotherapy and ICI combined therapy (Combination of 2 ICI drugs or ICI plus TKI) for advanced RCC at our institution.

	TKI monotherapy N = 39		ICI combination N = 30		P-value
sex	Male Female	32 (65.3%) 17 (34.7%)	Male Female	27 (90%) 3 (10%)	0.02
age	69 (43-86)		69 (35-84)		0.67
metastasis	M0 M1	33 16	M0 M1	11 19	0.01
pathology	Clear Cell Non-Clear Cell Unknown	31 (63.3%) 12 (24.5%) 6 (12.2%)	Clear Cell Non-Clear Cell Unknown	17 (56.7%) 7 (23.3%) 6 (20%)	0.72
IMDC risk group	Favorable Intermediate Poor	9 (18.4%) 34 (69.4%) 6 (12.2%)	Favorable Intermediate Poor	4 (13.3%) 15 (50%) 11 (36.7%)	0.05
T group	< T3 > T3	20 (40.8%) 29 (59.2%)	< T3 > T3	12 (40%) 18 (60%)	1.00
nephrectomy	Yes No Partial	41 (83.7%) 6 (12.2%) 2 (4.1%)	Yes No Partial	18 (60%) 11 (36.7%) 1 (3.3%)	0.03

Table1. Patient Backgrounds

Methods

- We conducted a study of patients who received first-line medical therapy for advanced RCC at our institution from April 2007 to November 2023.
- We evaluated and compared the outcomes of patients treated with TKI monotherapy and those treated with a combination of ICIs.
- Our evaluation included an analysis of progression-free survival (PFS), overall response rate (ORR) and overall survival (OS).
- The favorable and intermediate/poor risk groups were also analyzed separately by IMDC risk category for comparison.

Results

Patient Cohort

The study included a total of 79 cases, including 59 males and 20 females, with a median age of 69 years. Of these cases, 35 had evidence of metastases at the time of diagnosis and 44 had metastases at the time of treatment initiation. The distribution of the International Metastatic Renal Cell Carcinoma Database Consortium (IMDC) risk classification was as follows: favorable 16%, intermediate 62% and poor 21% (TKI group: 18% / 69% / 12%, ICI combination group: 13% / 50% / 37%). Notably, the ICI combined group had a higher prevalence of intermediate or higher risk patients. Renal surgery, either nephrectomy or partial nephrectomy, was performed in 62 cases, with 48 cases of clear cell RCC. There were no significant differences in the distribution of these characteristics between the two treatment groups. Regarding T stage, 32 cases were classified as T3 or higher, while 47 cases were classified as T3 or lower, and again, no significant differences were observed in the distribution between the two treatment groups.

Overall survival (OS)

In the overall study population, median OS in the TKI arm was 42.9 months (range: 16.7 months - 82.3 months), while it was not reached in the ICI combined arm (range: 22.5 months - NE). There was no statistically significant difference in OS between the two groups (p-value: 0.5) (Figure 1(A)). Similarly, there were no statistically significant differences in OS when stratified into favorable risk group and intermediate/poor risk groups (Figure 1(B)-(C)).

Progression-free survival (PFS)

Regarding PFS, the median PFS in the TKI group was 7.4 months (range: 4.8 months - 11.4 months), while in the ICI combined group it was 10.8 months (range: 6.9 months - NE), with a p-value of 0.08. This suggests a trend toward longer PFS in the ICI combined group, although it did not reach statistical significance. In the favorable risk group, no significant differences in PFS were observed. However, in the intermediate and poor risk groups, median PFS in the TKI arm was 7.1 months (range: 3.7 months - 10.8 months) compared to 10.8 months (range: 6.9 months - NE) in the ICI combination arm, with a statistically significant superiority favoring ICI combined therapy (p-value: 0.03).

Overall response rate (ORR)

In the overall study population, the ORR was 34.7% in the TKI arm and 63.3% in the ICI arm, with a statistically significant improvement in the ICI arm (p-value: 0.02). In the favorable risk group, the ORR was 44.4% in the TKI group and 75% in the ICI combined group, with no significant difference observed (p-value: 0.32). However, in the intermediate/poor risk groups, the ORR was 32.5% in the TKI group and 61.5% in the ICI combined group, with a statistically significant advantage in favor of ICI combined therapy (p-value: 0.02).

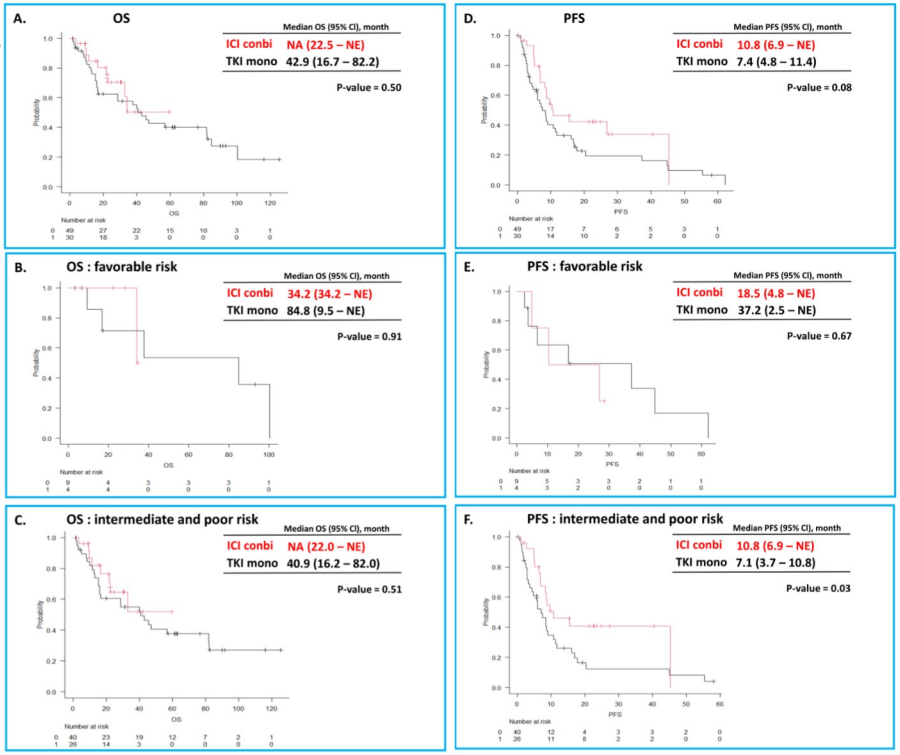

Figure 1 : (A) OS in all IMDC risk groups, (B) OS in favorable risk groups, (C) OS in intermediate and poor risk groups, (D) PFS in all IMDC risk groups, (E) PFS in favorable risk groups, (F) PFS in intermediate and poor risk groups.

Conclusions

- In the overall patient cohort, there was no statistically significant difference in overall survival (OS) and progression-free survival (PFS) between the TKI and ICI combination groups; however, a statistically significant difference in overall response rate (ORR) was observed.
- In the intermediate/poor risk groups, statistical significance was observed for both PFS and ORR.
- These results suggest that ICI combined therapy may be effective in real-world clinical practice, particularly in patients with intermediate and poor risk profiles[2].
- Although the efficacy of ICI combination therapy has been reported in the favorable risk group, this study had a limited number of cases. Therefore, further investigation with an expanded case cohort is warranted.

References

1) NCCN Clinical Practice Guidelines in Oncology, Kidney Cancer, Version 1. 2024; June 2023
2) Aly-Khan A Lalani, et al. *Ther Adv Med Oncol.* 2022, Vol. 14: 1-17

11

Development of models of Neurofibromatosis 2 (NF2) loss in kidney cancer of Hereditary Leiomyomatosis and Renal Cell Carcinoma (HLRCC)

Shinji Ohtake, MD[1,2]; Neal Patel, MD[1,3]; Lin Lin, MD PhD[1]; Blake Wilde, PhD[4]; Vitte Jeremie, PhD[5]; Randy Caliliw[1]; Heather Christofk, PhD[4]; Marco Giovannini, MD PhD[5]; Brian Shuch, MD[1]

1. Department of Urology, UCLA, Los Angeles, CA; 2. Department of Urology, Yokohama City University, Japan; 3. Department of Urology, Weill Cornell Medicine, New York, NY; 4. Department of Biological Chemistry, UCLA, Los Angeles, CA; 5.Department of Head and Neck Surgery, UCLA, Los Angeles, CA

Introduction

Hereditary Leiomyomatosis and Renal Cell Carcinoma (HLRCC) is characterized by cutaneous leiomyomas, uterine leiomyomas, and renal cell carcinoma, caused by a germline mutation in the Fumarate Hydratase (FH) gene.

HLRCC patients have aggressive disease with poor outcomes due to limited treatment options.[1,2]

Neurofibromatosis 2 (NF2) is an autosomal dominant disease mainly characterized by high risk of schwannomas.

NF2 mutations are identified in 15-20% of HLRCC kidney cancer.[3-5] As there has been extensive research on Neurofibromatosis-related cancers, we created models of the NF2 deficient HLRCC kidney cancer to assess the biologic effects and therapeutic sensitives to agents that have been investigated in this disease.

Materials & Methods

Three isogenic NF2KO cell lines were generated from NF2 wild-type HLRCC patients derived cell lines (NCCFH1, UOK262, and UOK268), using CRISPR.

Protein abundance was analyzed using Western Blot. Gene expression changes were evaluated using the Nanostring nCounter Tumor Signaling 360 gene expression panel and analyzed by ROSALIND™. Cell proliferation, soft agar, scratch wound-healing, and transwell invasion assay were performed.

Clonogenic survival assay, Cell proliferation and transwell invasion assay were performed in NF2KO HLRCC cell lines treated with Rapamycin, Everolimus, Brigatinib, GSK2256098, and TAK228.

Results

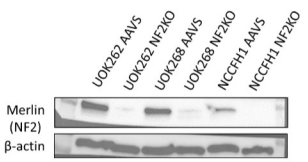

Figure 1: Western blot confirming CRISPR/Cas9 mediated KO of NF2. β-actin was used as a loading control.

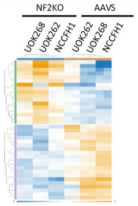

Figure 2: Gene expression changes were evaluated using the Nanostring nCounter Tumor Signaling 360 gene expression panel.

Results

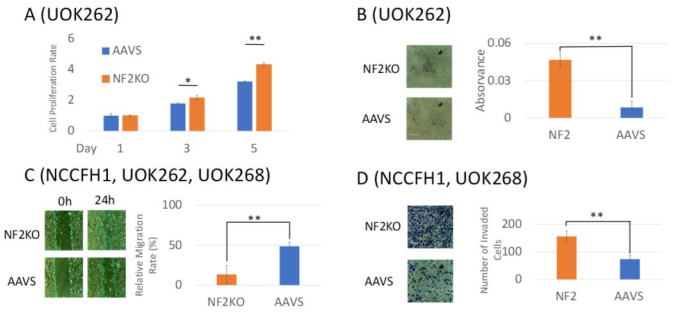

Figure 3: (A) Cell proliferation assay at 24, 72, and 120 hours (B) Soft agar assay (C) Scratch wound healing assay (D) Invasion assay. The names of cell line indicate that NF2KO in each cell line is significantly different than the control.

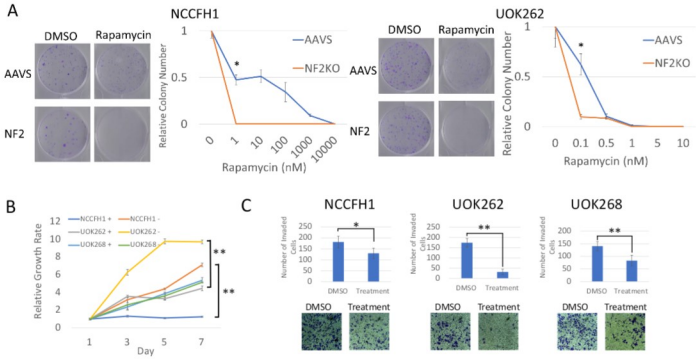

Figure 4: (A) Clonogenic survival assay of control vs NF2KO cells treated with a dose range of Rapamycin. Representative images (left panel) and quantification (right panel) (B) CyQUANT cell proliferation assay with 1uM Rapamycin. (C) Transwell cell invasion assay with 1nM Rapamycin.

Conclusions

Our current data indicated that FH deficient cell lines with NF2 loss of function may have more aggressive potential, and further suggest that mTOR complex-1 (mTORC-1) therapy could play a role into treatment algorithms of NF2 deficient HLRCC kidney cancers.

In vivo experiments are planned to further characterize the models and test therapeutic approaches.

References

1. Perrino, C. M., Grignon, D. J., Williamson, S. R. et al. Histopathology, 72: 305, 2018
2. Srinivasan, R., Gurram, S., Al Harthy, M. A. et al. J Clin Oncol, 38: no. 5004, 2020
3. Gleeson, J. P., Nikolovski, I., Dinatale, R. et al. Clin Cancer Res, 27: 2910, 2021
4. Sun, G., Zhang, X., Liang, J. et al. Clin Cancer Res, 27: 1734, 2021
5. Anderson, W. J., Tsai, H. K., Sholl, L. M. et al. Int J Surg Pathol, 30: 606, 2022

Funding

This work was supported by the Kidney Cancer Association

COI Disclosure Information

I have no COI with regard to our presentation.

12

LDH isozyme as a prognostic factor for patients with metastatic clear cell renal cell carcinoma

Hayato Takeda, Go Kimura, Mami Taniuchi, Ryota Funato, Hiroya Hasegawa, Hikaru Mikami, Jun Akatsuka, Yuki Endo, Yuka Toyama, Yukihiro Kondo

Nippon Medical School, Department of Urology

Introduction

LDH isozyme is a tetramer of two subunits, H chain and M chain, and is present in all living tissue. Five types of molecular forms characterize the LDH pattern.

Tumor tissues relatively consist LDH-4 and LDH-5, composed with a high ratio of the M chain, compared to normal tissues.

This study analyzed the association between LDH isozyme and prognosis of mCRCC after nephrectomy.

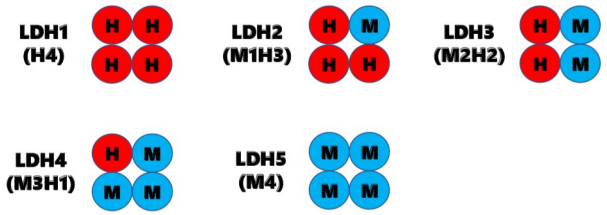

- LDH-1 (H4) : heart (at hypoxia), renal cortex & RBC
- LDH-2 (M1H3) : reticuloendothelial system
- LDH-3 (M2H2) : lung
- LDH-4 (M3H1) : liver, kidney, placenta, pancreas
- LDH-5 (M4) : liver, skeletal muscles

Material and Methods

Clinical records of metastatic clear cell carcinoma (mCRCC) patients those who were initially diagnosed M0 disease at Nippon Medical School between 2012 and 2016 were retrospectively reviewed.

LDH isozyme values before operation and at time of metastasis were checked. Isozyme patterns were classified into 6 types, LDH 1-5 dominant and common type, according to the most composed molecular form.

Results

Patient Characteristics

Patient background	Total n=38	
Age (median)	65 (36-87)	
sex	Male	33 (86.8%)
	Female	5 (13.2%)
pT stage	1	3 (7.9%)
	2	4 (10.5%)
	3	27 (71.1%)
	4	4 (10.5%)
Grade	2	9 (23.7%)
	3	21 (55.2%)
	4	8 (21.1%)
IMDC	Favourable	2 (5%)
	Imtermediate	26 (68%)
	Poor	10 (26%)

Pre-operative LDH isozyme dominant pattern

		Time to reccurence (M)
Serum LDH (median)	161 IU/l (118-294)	23.3 (1-104)
LDH-1	0 (0.0%)	*
LDH-2	3 (23.7%)	21.6
LDH-3	3 (15.8%)	18.8
LDH-4	2 (10.5%)	16.0
LDH-5	5 (28.9%)	14.2
Common type	25 (21.0%)	25.4

LDH isozyme dominant pattern at time of reccurence

		OS (M)	P value
Serum LDH (median)	163 IU/l (113-317)	18.0 (4-72)	
LDH-1	0 (0.0%)	*	*
LDH-2	9 (24.0%)	30.8	p=0.674
LDH-3	6 (16.0%)	24.3	p=0.579
LDH-4	4 (10.5%)	10.9	p=0.013
LDH-5	11 (28.9%)	20.5	p=0.154
Common type	8 (21.0%)	38.6	p=0.768

No significant correlation was seen between pre-operative LDH isozyme pattern and pathological grade or pT stage. Pre-operative LDH isozyme did not correlate with the time to recurrence (p=0.742). The median OS for LDH-4 dominant at the time of metastasis was 10.9 months, significantly shorter than other isozyme types.

Discussion

Cancer cells undergo a metabolic shift towards anaerobic glycolysis, increasing the production of lactate, which is then converted to pyruvate by LDH-5. The resulting increase in pyruvate levels can support the growth and proliferation of cancer cells.

Last step of Anaerobic Glycolysis

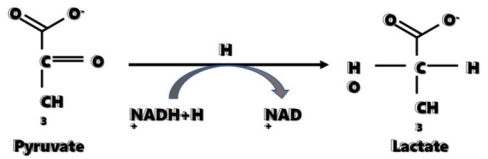

LDH-4 plays a critical role in energy metabolism.

It is primarily found in liver tissue, and its evaluation in cancer patients can be linked to liver metastases. (presense of liver metastases is associated with a poorer prognosis)

LDH-4 can also be targeted for cancer treatment. Small molecule inhibitors of LDH block the conversion of lactate to pyruvate, leading to a buildup of lactate that can inhibit cancer cell growth and induce cell death.

Normal levels of LDH show an improved overall survival when treated with immune checkpoint target therapies, and elevated LDH levels is significantly associated with poor progression free survival.

Conclusion

LDH-4 dominant isozyme pattern at time of recurrence has a short OS, proposing as a prognostic predictor in mRCC.

COI Disclosure information

I have no COI with regard to my presentation.

13

Elucidation of Transcriptional regulation in Translocation Renal Cell Carcinoma Using CRISPR/Cas9 Genome-Wide Screening

Hidekazu Nishizawa[1,2], Shintaro Funasaki[2], Ryoma Kurahashi[1], Takuya Segawa[1], Takanobu Motoshima[1], Yoji Murakami[1], Junji Yatsuda[1] , Masaya Baba[2] , Tomomi Kamba[1]

1)Dept. of Urology, Grad. School of Med. Sci., Kumamoto University 2)Laboratory of Cancer Metabolism, IRCMS, Kumamoto University

Kumamoto University

Abstract

Objective: Xp11.2 translocation renal cell carcinoma (Xp11.2 tRCC) is a type of renal cell carcinoma caused by the formation of a fusion gene through translocation on the X chromosome, resulting in the constitutive activation of the transcription factor TFE3. We demonstrated the ability of the fusion TFE3 (PRCC-TFE3) to induce renal cell carcinoma through the creation of kidney-specific PRCC-TFE3-expressing mice. However, fusion TFE3 also induces an Oncogene-induced senescence (OIS)-like cell growth inhibition in human renal proximal tubule-derived HK2 cells and human embryonic kidney-derived HEK293 cells. This study aims to elucidate the transcription mechanism of the oncogene fusion TFE3 by identifying the genetic changes necessary for cell growth inhibition induced by fusion TFE3 using CRISPR/Cas9 genome-wide screening.

Methods: We established stable CRISPR/Cas9-expressing HK2 cell lines with inducible PRCC-TFE3. Genome-wide screening using an sgRNA library was conducted in these HK2 cells, and candidate genes were evaluated through RNA sequencing, ChIP qPCR, and immunostaining.

Results: CCNC was identified as an essential gene for cell growth inhibition induced by fusion TFE3 expression. CCNC is a constituent factor of the mediator complex that regulates transcription. Inhibition of the mediator complex by treatment with its inhibitor led to a suppression of cell growth inhibition similar to CCNC KO in response to fusion TFE3 expression. Furthermore, treatment with the mediator complex inhibitor revealed selective control of fusion TFE3 transcriptional activity. ChIP qPCR and immunostaining using CCNC antibody also suggested that the mediator complex selectively regulates fusion TFE3 transcriptional activity.

Conclusion: This study reveals that the transcriptional activity induced by the oncogene fusion TFE3 is selectively controlled by the mediator complex. The mediator complex emerges as a potential novel therapeutic target for Xp11.2 translocation renal cell carcinoma.

Introduction

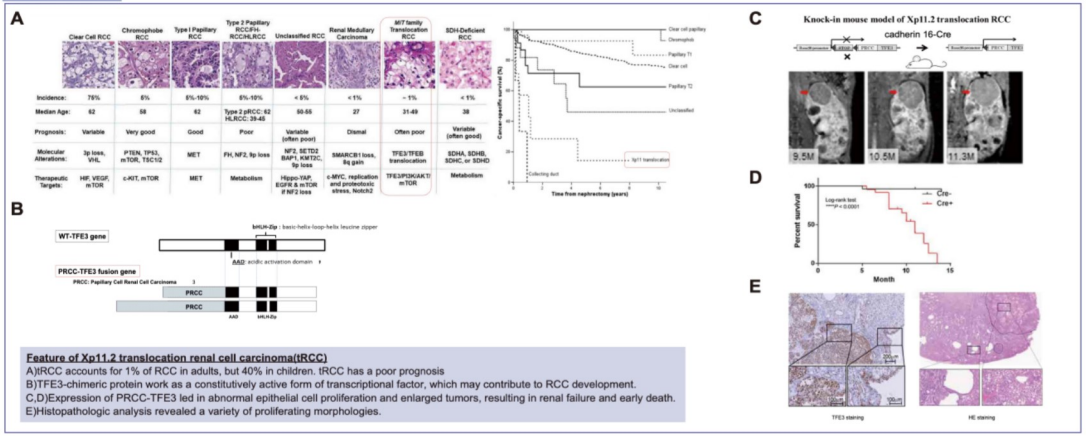

Feature of Xp11.2 translocation renal cell carcinoma(tRCC)
A)tRCC accounts for 1% of RCC in adults, but 40% in children. tRCC has a poor prognosis
B)TFE3-chimeric protein work as a constitutively active form of transcriptional factor, which may contribute to RCC development.
C,D)Expression of PRCC-TFE3 led in abnormal epithelial cell proliferation and enlarged tumors, resulting in renal failure and early death.
E)Histopathologic analysis revealed a variety of proliferating morphologies.

1.PRCC-TFE3 induces OIS and suppresses proliferation at G0/G1

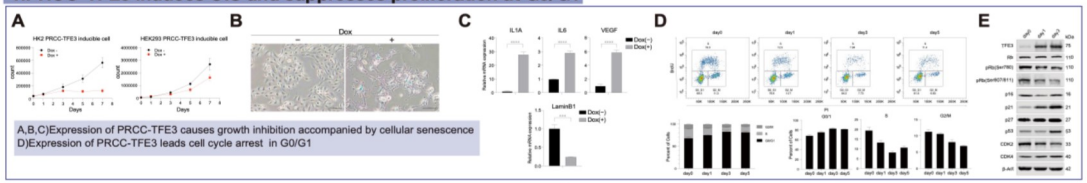

A,B,C)Expression of PRCC-TFE3 causes growth inhibition accompanied by cellular senescence
D)Expression of PRCC-TFE3 leads cell cycle arrest in G0/G1

2.Extraction of CCNC by CRISPR Cas9 genome wide screening

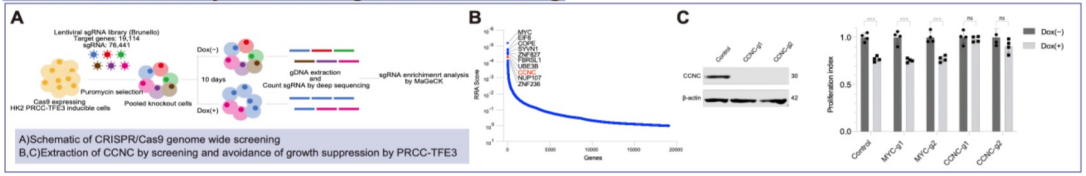

A)Schematic of CRISPR/Cas9 genome wide screening
B,C)Extraction of CCNC by screening and avoidance of growth suppression by PRCC-TFE3

3.CCNC KO rescues from growth inhibition and OIS by PRCC-TFE3

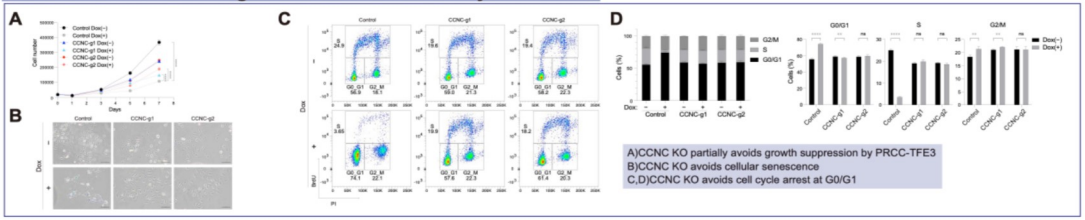

A)CCNC KO partially avoids growth suppression by PRCC-TFE3
B)CCNC KO avoids cellular senescence
C,D)CCNC KO avoids cell cycle arrest at G0/G1

4.CDK8/19 inhibition rescues from growth inhibition and OIS by PRCC-TFE3

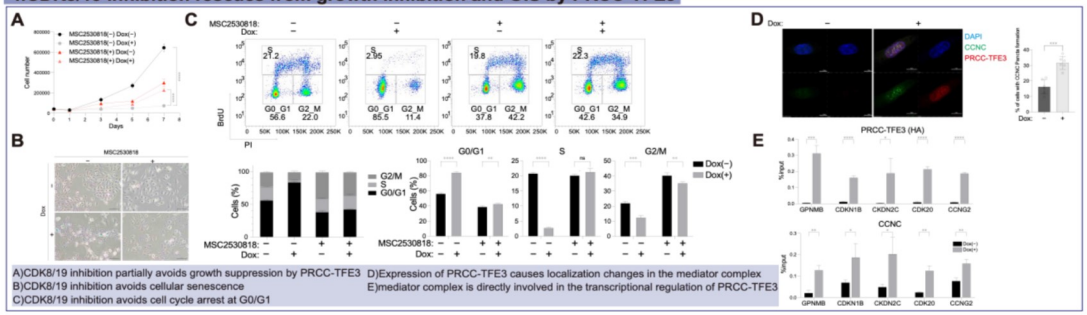

A)CDK8/19 inhibition partially avoids growth suppression by PRCC-TFE3
B)CDK8/19 inhibition avoids cellular senescence
C)CDK8/19 inhibition avoids cell cycle arrest at G0/G1
D)Expression of PRCC-TFE3 causes localization changes in the mediator complex
E)mediator complex is directly involved in the transcriptional regulation of PRCC-TFE3

5.Transcriptional regulation by PRCC-TFE3 requires mediator complex function

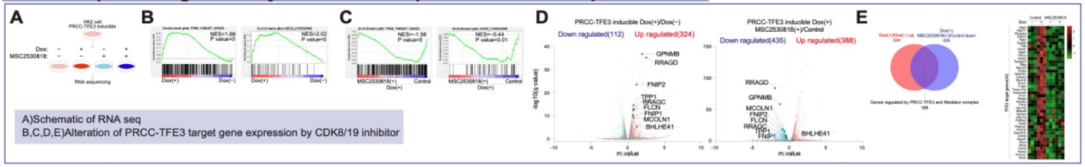

A)Schematic of RNA seq
B,C,D,E)Alteration of PRCC-TFE3 target gene expression by CDK8/19 inhibitor

Conclusion

In this study, we conducted a genome-wide screening using the CRISPR/Cas9 system and identified CCNC as a critical gene responsible for oncogene induced senescence by fusion TFE3. CCNC is an essential component of the mediator complex. Furthermore, we have uncovered a novel finding that the mediator complex selectively associates with the specific transcriptional activity of fusion TFE3. This discovery may offer potential insights into novel therapies for tRCC.

COI Disclosure Information

Lead Presenter/Principal Researcher:
Hidekazu Nishizawa

I have no financial relationships to disclose.

14

Which affects nocturnal frequency most: Urgency or sleep disorders?

Okumura Y. , Masaya Seki, Sou Inamura, Minekatsu Taga, Fukushima M. , Aoki Y. , Ito H. , Yokoyama O. Department of Urology, University of Fukui, Fukui, Japan

【Introduction】

- There are three major causes of nocturia: bladder storage dysfunction, nocturnal polyuria, and sleep disorders.
- Although the majority of patients with nocturia have nocturnal polyuria, we have found no reports regarding whether bladder storage or sleep disorders contribute more strongly to nocturnal voiding frequency.
- We analyzed whether urinary urgency or sleep disorders more strongly affects nocturnal frequency.

【Methods】

- We analyzed the symptom severity of male patients with LUTS /BPH at their first visits to our outpatient department between April 2014 and May 2018.
- Patients were evaluated on their International Prostate Symptom Score (IPSS) and and a self-assessment sleep quality questionnaire (Quality of Sleep Score; QOSS), which rated sleep quality on a 5-point scale (1: very good - 5: very poor).

QOSS (Question : How was your quality of sleep ?)				
1	2	3	4	5
Very good	good	Not good or bad	bad	Very bad

- The participants were divided into two groups based on the median score of IPSS question 7, which pertains to nocturia frequency: nocturia ≤ 2 times and nocturia ≥ 3 times. We compared IPSS questions 1-6 and QOSS scores between the two groups.

【Results】

A total of 1018 out of 1478 eligible individuals (mean age: 72.9 ± 9.5 years) were included in the study.

*average

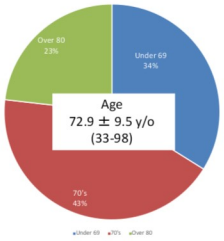

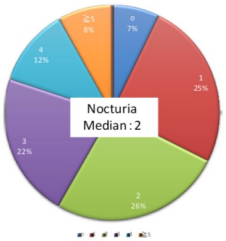

【Univariate and multivariate statistics and forest plot.】

	Univariate statistics			Multivariate statistics			
	nocturia				95% CI		
	≤2 (n=425)	≥3 (n=593)	P values	OR	lower	upper	P values
IPSS-q1 (Imcomplete emptying)	1.38	2.34	<0.001	1.08	0.97	1.19	NS
IPSS-q2 (Frequency)	1.82	3.25	<0.001	1.28	1.15	1.43	<0.001
IPSS-q3 (Intermittency)	1.51	2.35	<0.001	0.97	0.87	1.08	NS
IPSS-q4 (Urgency)	1.07	2.51	<0.001	1.37	1.23	1.51	<0.001
IPSS-q5 (Weak stream)	2.09	3.2	<0.001	1.08	0.97	1.19	NS
IPSS-q6 (Straining)	1.26	1.91	0.011	0.93	0.84	1.03	NS
QOSS (Quality of sleep)	2.53	3.4	<0.001	1.76	1.53	2.03	<0.001

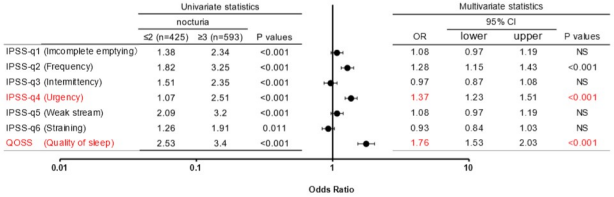

- In univariate analysis, the results were significantly higher in all items in the group with nocturia 3 times or more than in the group with 2 times or less.
- In multivariate statistics, urinary urgency and poor sleep quality were significant association factors for nocturia.
- Odds ratio of sleep quality was highest (1.76; p value<0.001).

【Comparison of each age group】

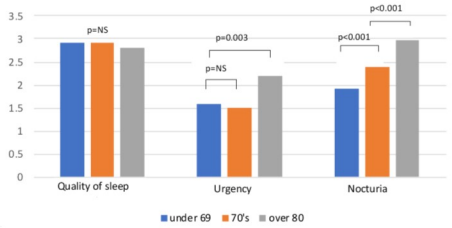

- There was no difference in sleep quality between the three groups.
- Urgency was strongest in the over 80 group.
- There was no difference in sleep quality between the three groups.
- Urgency was strongest in the over 80 group.
- Nocturia gradually increased by age group.

【Conclusions】

- This study suggested that poor sleep quality and urinary urgency were both significant factors associated with nocturia.
- It was also suggested that poor sleep quality was the strongest association factor for those aged 79 years and younger, while urgency was the only significant association factor for those aged 80 years and older.

The 110th Annual Meeting of the Japanese Urological Association
COI Disclosure Information
Yoshinaga Okumura

15

Two-photon calcium imaging uncovered that micturition-related neural activity in the cerebral cortex depends on the location, cell-type, and projection pathway

Shimura H.[1] , Manita S.[2] , Mochizuki T.[1] , Matsuda Y.[1] , Aikawa J.[1], Kira S.[1] , Sawada N.[1], Takeda M.[1], Kitamura K.[2] ,Mitsui T.[1]

1. University of Yamanashi Graduate School of Medical Sciences, Department of Urology
2. University of Yamanashi Graduate School of Medical Sciences, Department of Neuroscience

University of Yamanashi

Introduction and Object

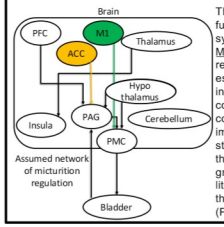

The regulation of lower urinary tract function by the central nervous system is a complex process. Micturition-related neural activity remains poorly understood, especially in the cerebral cortex including the anterior cingulate cortex (ACC) and the primary motor cortex (M1). ACC must have important role in micturition (also in storage phase) and assumed to be the pathway to the periaqueductal gray matter (PAG). In the past literature, M1 has the pathway to the pontine micturition center (PMC).

Calcium imaging

In recent years, neural activity is often assessed using calcium imaging, which is a microscopy technique to optically measure the neural activity-dependent changes in intracellular calcium (Ca^{2+}) concentration. Genetically-encoded calcium indicators (GECIs) have provided large advantages of high spatiotemporal resolution and cell-type specific recordings by labeling of specific neurons according to the neuronal types or the circuits.

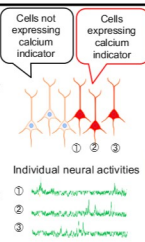

Two-photon calcium imaging

ACC plays important roles for a number of different functions, e. g., pain, emotion, cognition, decision making, and motor control. Distinct type of neurons in ACC would have different roles in a certain behavior, and recording micturition-related neural activity in ACC requires single cell resolution with cell-type specificity. We took advantage of two-photon calcium imaging for resolving spatial distribution of recorded neurons at single cell resolution. Moreover, two-photon calcium imaging enables less invasive observation (No need to insert fibers for ACC and M1).

Object

In this study, we observed the neural activities in ACC and M1 of mice during micturition to uncover the distribution and functional properties of micturition-related neurons. Two-photon calcium imaging would provide new findings that offer the foundation for investigating the pathophysiology of regulating micturition.

Methods

Outline of method

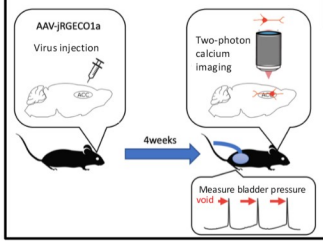

After virus (expressing GECIs) injection for target region (ACC or M1), two-photon calcium imaging was performed during bladder perfusion under urethane anesthesia. Micturition timing was identified by developed detection device.

Targeted cortical regions and cell-types

regions: ACC and M1

cell types:
A) non-selectively labeled neurons
B) layer 5 pyramidal neurons
C) neurons projecting to certain regions; ACC to PAG or M1 to PMC.

Mice and injected viral vectors

A) WT and red calcium indicators (jRGECO1a)
B) $Rbp4^{Cre}$ mice and flex-NES-jRGECO1a
C) WT and flex-NES-jRGECO1a at the origins of the projection (ACC or M1) , AAV-retrograde-Cre at the projection targets (PAG or PMC)

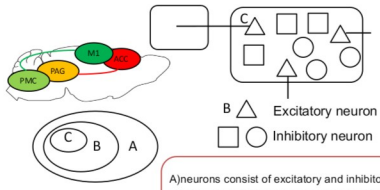

A)neurons consist of excitatory and inhibitory neurons and B)neurons are excitatory neurons. Because excitatory cerebral cortex neurons project other regions, C) is included in B).

Two-photon calcium imaging

We took advantage of two-photon calcium imaging for high spatial resolution and less invasive observation.

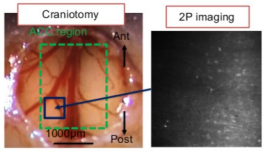

After craniotomy on targeted region, two-photon calcium imaging was performed during micturition cycles with head fixation under urethane anesthesia.

Micturition cycles were repeated for 30 min during one imaging session, and the cycle intervals were approximately 3 min. Three planes were acquired in one session. A 30 min session was repeated several times with changing the imaging location.

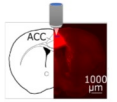

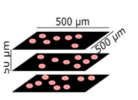

Evaluation

Representative extracted micturition-related neuron

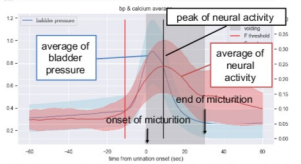

After the process of imaging from acquired data, we extracted micturition-related neurons using specific programming; The timing of the peak activity during micturition is less than 5% of the standard deviation of the shuffle data, based on the onset of micturition.

We examined the percentage and localization of micturition-related cells for each cell-type. The distribution of latency of activity peaks was also examined for each.

Results

Representative data of neural activities

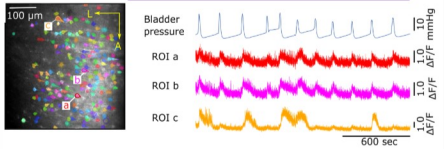

Left; Representative two-photon image of non-selective neurons in ACC. In one imaging plane, 100-200 cells are detected. Right; Representative fluorescence signals from right image with bladder pressure during one session (30min). Neural activities of ROI a and b are well synchronized with micturition. Neural activity of ROI c is not synchronized with micturition.

Representative extracted micturition-related neuron

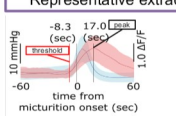

Representative micturition-related neural activity (ROI a). Red curve line; averaged fluorescence signal. Blue curve line; averaged bladder pressure.

Color plot of neural activities from one observed view

Right color plot represents all observed neural activities in one representative FOV (from left representative data) (neurons = 236). Each fluorescence signal was normalized. Dark blue is low and light yellow is high signal. Magenta square are extracted 30 neurons as micturition-related.

Thus, there is a mixture of micturition-related and other cells within the same observed region.

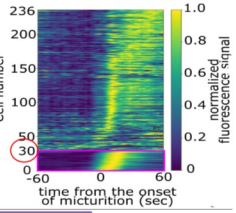

The percentage of micturition-related neurons

region	cell-type pattern	n (mice)	all neurons	micturition -related neurons	ratio of micturition-related neurons (%)
ACC	non-selective	4	18,213	1,154	6.34
	layer 5 pyramidal	3	13,164	1,444	10.97
	projection to PAG	4	2,283	215	9.42
M1	non-selective	4	24,068	1,591	6.61
	layer 5 pyramidal	3	12,099	1,250	10.33
	projection to PMC	4	2,861	243	8.50

The population of micturition-related neurons is only a part of the whole ACC or M1 neurons (6 ~10%). The percentage of micturition-related cells within the observation region is the same for both ACC and M1.

Heat maps of the ratio of micturition-related neurons

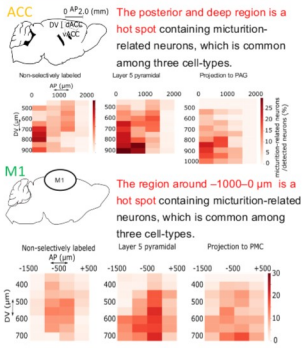

ACC: The posterior and deep region is a hot spot containing micturition-related neurons, which is common among three cell-types.

M1: The region around −1000–0 μm is a hot spot containing micturition-related neurons, which is common among three cell-types.

The peak timing of micturition-related neural activity depends on the location, cell-type, and projection pathway in ACC.

In the histograms of the peak latency regarding ACC, we found that peak latency of all (non-selectively labeled) neurons showed a broad distribution while layer 5 pyramidal neurons consisted of two different populations, early and delayed peak neurons.

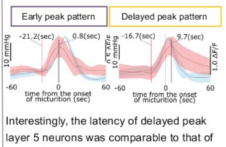

Interestingly, the latency of delayed peak layer 5 neurons was comparable to that of the PAG projecting neurons. Thus, micturition-related delayed peak layer 5 pyramidal neurons in ACC are presumably PAG projecting neurons.

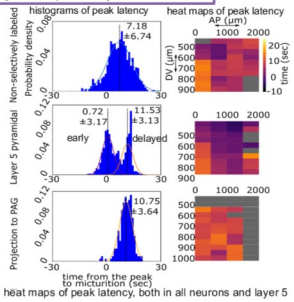

From heat maps of peak latency, both in all neurons and layer 5 pyramidal neurons, the timing in posterior and deep region was delayed compared with that in other regions. However, all ACC neurons projecting to PAG showed delayed peak latency irrespective of the location.

The timing of micturition-related neural activity is uniform throughout M1

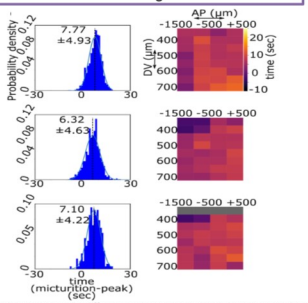

We found no systematic differences between neuronal types examined in both latency histograms and heat maps in M1.

Therefore, the activity pattern in M1 would be common in any cell-type and projection pathways.

Discussion & Conclusion

ACC may have multi-functional clusters regarding micturition, depending on their location, cell-type, and projection pathway.

M1 may have single functional cluster well synchronized with bladder pressure.

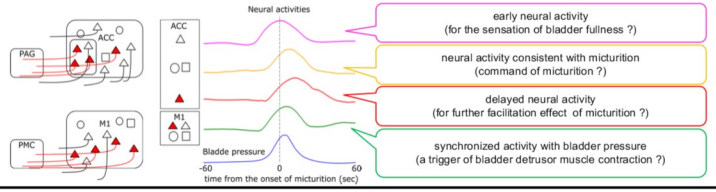

We detected micturition-related activities of individual neurons in the cerebral cortex with high spatial resolution and cell-type specificity. This is the first study using two-photon calcium imaging for the investigation of micturition and demonstrating the variety of micturition-related neuronal activity in the cerebral cortex.

Cerebral cortex neurons have multi-functional properties depending on the location, cell-type, and projection pathway.

Utilizing this calcium imaging method would uncover the mechanism of micturition in the future.

Advancements in Urology 2024
COI Disclosure Information
Hiroshi Shimura

Matters requiring disclosure of COI with regard to our presentation are as follows.

Reseach founding:JSPS KAKENHI Grant Number 20K18135, JP22K09496, Grant for Young Researcher from Yamanashi Prefecture, Young Research 108 Grant from the Japanese Urological Association and GSK Japan Research Grant 2021

16

Decreased NO Production and Increased Arteriosclerosis Cause Salt-induced Nocturnal Polyuria.

Takahiro Imanaka, Hiroaki Kitakaze, Go Tsujimura, Sohei Kuribayashi, Norichika Ueda, Kentaro Takezawa, Shinihiro Fukuhara, Norio Nonomura

Department of Urology, Osaka University Graduate School of Medicine

Background and objective

Nocturnal polyuria is the most common cause of nocturia, accounting for 67% to 88% of all nocturia cases[1]. Nocturia is not only a troublesome symptom that affects quality of life but also affects mortality[2].
However, no fundamental treatment against nocturnal polyuria has been established, because the pathogenesis of nocturnal polyuria is complex and not well understood. Previously, we have reported that a combination of nitric oxide (NO) deficiency and high salt intake induces nocturnal polyuria in mice[3]. We hypothesized that the same mechanism may cause nocturnal polyuria in humans. The abdominal aortic calcification index (ACI), a measure of abdominal aortic calcification, was reported to decrease NO production from arterial endothelium. We hypothesized that ACI is a predictor of salt-induced nocturnal polyuria in humans.

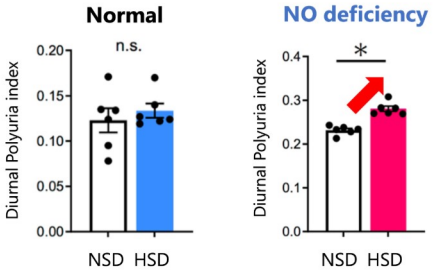

NSD : Normal salt diet
HSD : High salt diet

The objectives of this study were to elucidate the effects of decreased NO production on salt-induced nocturnal polyuria and evaluate the predictive value of ACI for salt-induced nocturnal polyuria in humans.

1. Van Doorn B, et al., Eur Urol, 2013
2. Funada S, et al., J Urol, 2020
3. Sekii Y, et al., Commun biol, 2022

Study design, Subjects and Methods

Subjects

Living kidney transplantation donors between June 2019 and October 2020

Study 1. The effects of NO production on salt-induced nocturnal polyuria

The patients were admitted to our hospital 2-4 days before surgery, and twenty-four-hour urine collection tests were performed 2 days before surgery. The Urine collected from 10:00 to 22:00 h was defined as daytime urine and urine from 22:00 to 10:00 h as nighttime urine. The daytime and nighttime urine volume, urinary salt excretion, and urinary nitric oxide (NOx) excretion were evaluated. The nighttime urine volume rate was defined as nighttime urine volume/daily urine volume. The urinary salt excretion was regarded as salt intake. The patients were classified into two groups, high NOx and low NOx group, according to the amount of NOx excretion. The correlation between salt intake and nighttime urine volume rate was compared between the two groups.

Study 2. The predictive value of ACI for salt-induced nocturnal polyuria

The arteriosclerosis was evaluated by abdominal calcification index (ACI) [1]. All patients were scanned using a non-contrast CT scan with a 5-mm slice thickness. Calcification was considered to be present if an area of >1mm2 displayed a density of >130 Hounsfield units. cross-section of the abdominal aorta on each slice was radially divided into 12 segments. The ACI was calculated as follows: ACI = (t score for calcification on all slices)/12 x 1/ (number of slices) x 100%. First, the patients were classified into two groups, high ACI and low ACI group, according to the ACI. The NOx excretion was compared between the two groups. Next, the correlation between salt intake and nighttime urine volume rate was compared between the two groups.

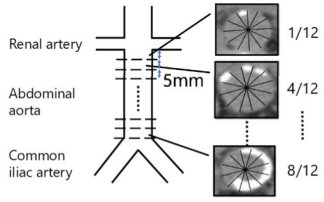

ACI = mean of calcification scores

1. Tatami Y et al., Atherosclerosis, 2015

First, the patients were classified into two groups, high ACI and low ACI group, according to the ACI. The NOx excretion was compared between the two groups. Next, the correlation between salt intake and nighttime urine volume rate was compared between the two groups.

Results

1. The effects of NO production on salt-induced nocturnal polyuria

Characteristics of patients (n=27)

Age, year	61 (42-79)
Men, n	10 (37%)
Height, cm	160 (148-175.5)
Weight, kg	61.8 (45.9-78.9)
BMI, kg/m^2	24.0 (18.0-27.8)
eGFR, mL/min/1.73m^2	76.5 (48.6-98.8)
Salt intake, g	6.6 (2.8-15.4)
Urinary NOx excretion, umol/Cr mg	0.26 (0.02-0.59)
ACI, %	3.3 (0-27.4)

median (range)

Correlation between salt intake and nocturnal urine volume rate

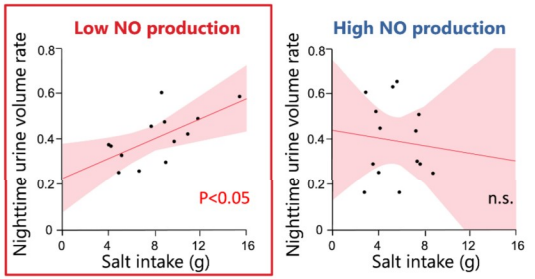

A positive correlation was observed in the Low NO production group.

2. The predictive value of arteriosclerosis for salt-induced nocturnal polyuria

Relationship between ACI and NO production

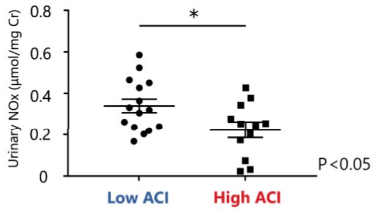

Predictive value of ACI for salt-induced nocturnal polyuria

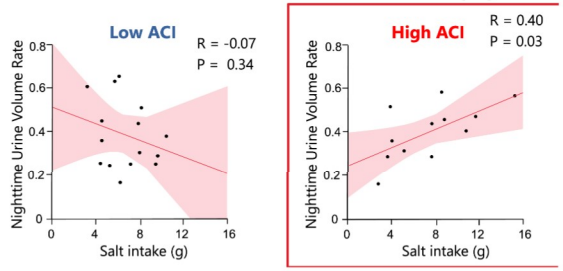

NO production was significantly lower in High ACI group.

A positive correlation was observed in High ACI group.

Conclusions

We found that decreased NO production and increased arteriosclerosis caused salt-induced nocturnal polyuria in humans.
ACI predict salt-induced nocturnal polyuria in humans.

Advancements in Urology 2024

COI Disclosure Information

Tkahiro Imanaka

I have no COI with regard to our presentation.

17

Creatine chemical exchange saturation transfer imaging (Cr-CEST) is an innovative method for evaluating intratesticular spermatogenesis.

Sohei Kuribayashi[1], Shinichiro Fukuhara[1], Hiroaki Kitakaze[1], Go Tsujimura[1], Takahiro Imanaka[1], Norichika Ueda[1], Kentaro Takezawa[1], Shigeyoshi Saito[2], Hidetaka Kioka[3], Masahito Ikawa[4], Norio Nonomura[1]

1. Department of Urology, Osaka University Graduate School of Medicine 2. Department of Medical Physics and Engineering, Osaka University Graduate School of Medicine
3. Department of Cardiovascular Medicine, Osaka University Graduate School of Medicine 4. Research Institute for Microbial Diseases, Osaka University

Background and objective

- The sperm retrieval rate in non-obstructive azoospermia (NOA) is still insufficient. To overcome this problem, an accurate noninvasive method of evaluating testicular spermatogenesis is needed[1].
- Chemical exchange saturation transfer (CEST) imaging is a new magnetic resonance imaging (MRI) technique that can image the distribution of trace substances in vivo[2].
- By targeting the protons of low-concentration compounds other than water and fat with a long duration of specific saturation pulses, the concentration of the target molecule can be detected as a decrease in the signal of water molecules.

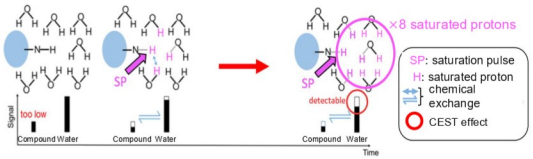

- Creatine (Cr) in the testes is decreased in patients with Klinefelter syndrome and NOA patients[3,4]. We focused on the Cr levels in testes and hypothesized that Cr-CEST could indicate intratesticular spermatogenesis noninvasively.
- The purpose of the present study was to develop a new noninvasive method of assessing intratesticular maturity using Cr-CEST.

1. Yumura Y, et al. ***Reprod Med Biol.*** 2018 2. Klostranec JM, et al. ***Radiology.*** 2021
3.Alves MG et al. ***Mol Reprod Dev.*** 2016 4.Storey P. ***Invest Radiol.*** 2018

Conclusions

- We found that Cr-CEST evaluates intratesticular spermatogenesis both qualitatively and spatially.
- Cr-CEST is a useful and novel noninvasive method for assessing maturity in the testis.
- Cr-CEST is a feasible and promissive method for preoperative imaging for evaluating intratesticular spermatogenesis and a navigation system during microscopic testicular sperm extraction.

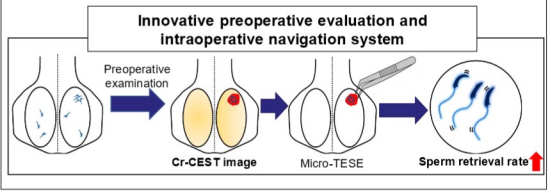

Methods

- All image processing and data analysis was performed with in-house scripts written in MATLAB.
- SXppm is defined as the signal intensity obtained by sequence with saturation pulse at Xppm.
- The CEST signal intensity was evaluated using magnetization transfer ratio (MTR) asymmetry analysis, determined from the following equation:

$$MTR_{asym} = (S_{-1.8ppm} - S_{1.8ppm}) / S_0$$

- The frequency of the saturation pulse is how far away from the frequency of the water molecule, in units of ppm.
- The Cr-CEST effect was evaluated at 1.8 ppm based on the phantom study (Cr solution).
- We used Z-spectrum which is a plot of the water signal level versus off-resonance saturation frequency.

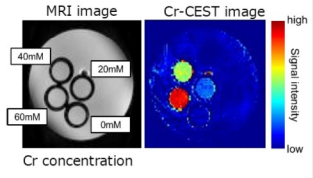

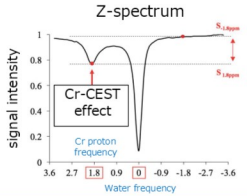

Study 1. Cr-CEST of male Infetility model.

- We performed Cr-CEST in male infertility models mice (the Sertoli-cell-only syndrome model (SCO), and the maturation arrest model (MA)) and in the wild type mice (C57BL/6J) (n=3, 6 testes per group).
- We used *Kit*^{w}/*Kit*^{wv} mice as a model for SCO which lacks germ cells and shows only Sertoli cells in the seminiferous tubules.
- We used *Kctd19* KO mice as a model for MA which stopped maturation at metaphase I.
- All mice underwent Cr-CEST imaging at 4 weeks of age because the testes of male infertility model mice atrophy considerably after 4 weeks of age.

Study 2. Cr-CEST of partial irradiation model.

Three mice (10 weeks of age) were subjected to X-ray irradiation localized to the lower regions of the testes by shielding the upper testicular regions with a lead plate.
Cr-CEST was performed 30 days after irradiation, and testicular samples were obtained from the testes 30 days after irradiation (n = 12 sections from 6 testes).

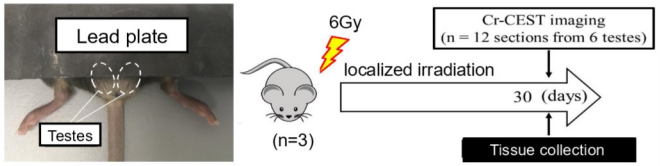

Results

1. Cr-CEST of male Infertlity model.

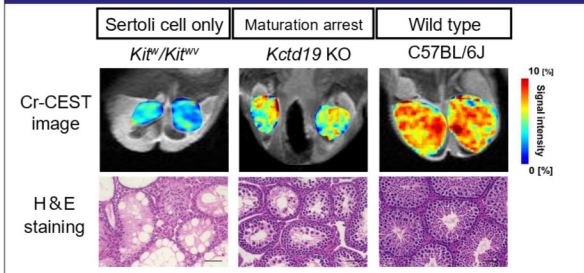

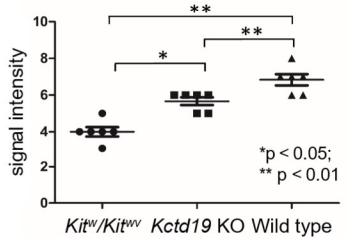

✓ **Cr-CEST signal intensity was increased as maturation in the testes progressed in the order of Sertoli cell only, Maturation arrest, and wild type.**

2. Cr-CEST of Partial Irradiation model.

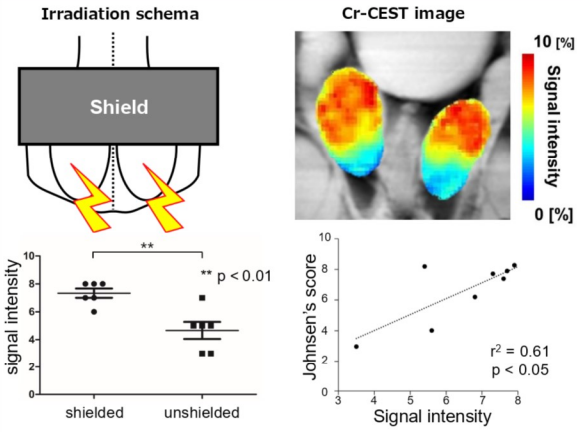

✓ **Irradiated areas showed vacuolation of seminiferous tubules and loss of germ cells compared to non-irradiated areas.**
✓ **Cr-CEST signal intensity in the irradiated area was significantly lower than that in the non-irradiated area.**

Summary of results

- In the male infetility and partial radiation models, Cr-CEST signal intensity showed a decrease consistent with testicular maturity.
- Cr-CEST was consistent with testicular maturity and allowed noninvasive imaging of spermatogenesis.

Advancements in Urology 2024
COI Disclosure Information

Sohei Kuribayashi

I have no financial relationships to disclose.

18

Isolated calyx caused by robot-assisted partial nephrectomy for neuroendocrine tumor of horseshoe kidney: A case report

Kobayashi K. , Wada A, Yoshida T. Johnin K. , Kageyama S.
Shiga university of medical science, The department of urology, Otsu, Japan

Introduction

Robot-assisted partial nephrectomy (RAPN) has become a standard treatment option for the management of small renal tumors. Surgical assistance robots have enabled us to perform more challenging RAPN procedures that would have otherwise been impossible. While surgical assistance robots have expanded the implementation of partial nephrectomy (PN) surgeries, these procedures can lead to complications that are rarely caused by conventional PN. One potential complication is an isolated calyx which involves the disconnection of the renal calyx and pelvis.

Renal neuroendocrine tumors (NETs) are low-grade tumors with neuroendocrine differentiation, and NETs in the kidney are extremely rare.

We present a case of NET in a horseshoe kidney with an isolated calyx caused by robot-assisted partial nephrectomy.

Case

Case : A 56-year-old man
Complaints : Left renal tumor
History : Splenic Hamartoma, Hypertension, Hyperlipidemia, Myocardial infarction, Depression

The patient was pointed out a left renal tumor incidentally and was referred to our hospital.

There were no significant findings in blood and biochemistry tests.

Contrast-enhanced CT

CT revealed a horseshoe kidney and a hypovascularized tumor with a diameter of 19 mm in the ventral side of the left kidney hilum.

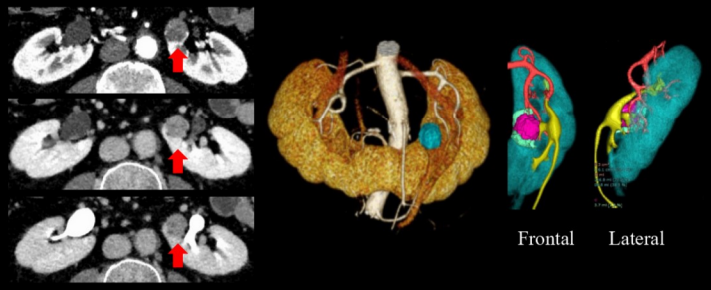

Laparoscopic Partial Nephrectomy

Off-clamp RAPN was performed. The tumor was easily identified(A) and exposed. After excising the tumor, we found that the renal pelvis was open (B) and closed it using a running suture. However, there was persistent urine leakage from the resection site. We then found a renal papilla that was located some distance from the renal calyx at the resection site, and they were too far apart to anastomose (C).

The renal papilla was therefore coagulated to prevent postoperative urine leakage(D). The total operative time was 333 min and total blood loss was 50 ml. The postoperative recovery period was uneventful.

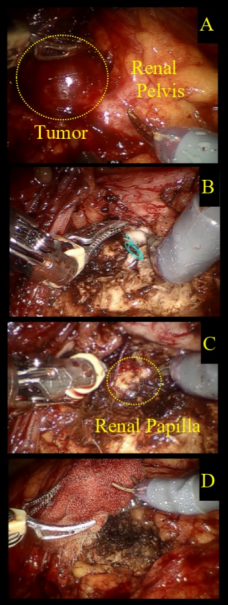

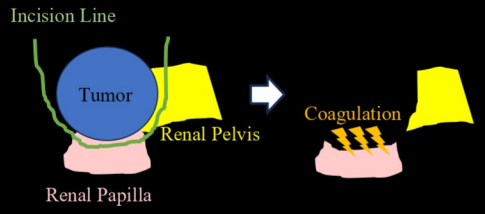

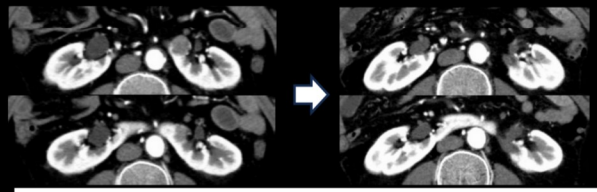

Histological Finding

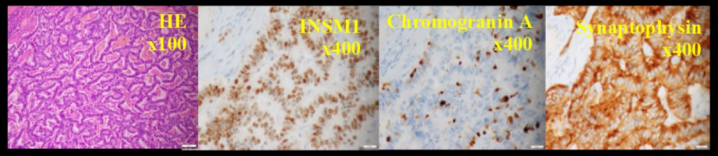

Discussion: Isolated Calyx

An isolated calyx is a rare but troublesome complication causing persistent urinary fistula, and the treatment is often complicated. Isolated calyx would be often unavoidable. The renal papilla was therefore coagulated to prevent postoperative urine leakage in our case. Coagulation of renal papilla could minimize loss of renal function due to limited area for procedure(A).

TAE is one treatment option for persistent urinary fistula caused by isolated calyx discovered postoperatively.

However, TAE may cause a greater reduction in renal function(B).

We should note the occurrence of isolated calyx in partial nephrectomy for renal hilum tumors.

Intraoperative detection has a possibility to prevent postoperative complications and minimize the decline in renal function.

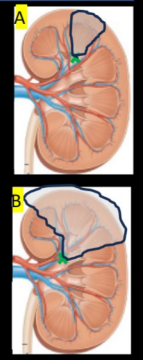

Discussion: Neuroendocrine tumor (NET) in Kidney

NETs in the kidney are extremely rare.

NET are thought to arise from neuroendocrine cells (NECs). However, NECs are not found within normal renal parenchyma. So many hypotheses have been proposed for the coexistence of primary renal neuroendocrine tumors. The most popular hypothesis is the totipotent cell hypothesis, that primary renal neuroendocrine tumor arises from multipotential stem cells.

The primary renal NET have been reported to arise most commonly in the setting of congenital renal abnormalities. Relative risk of NET in HSK are reported 62-120 versus NET in normal kidney , considering an incidence of HSK in the general population of 1:400.

The prognosis of NETs is still a debatable issue, due to the rarity of the disease. The stage of the disease seems to be the most important prognostic factor. A review of the reported cases, however, suggests a better prognosis of NETs in HSK than in those arising in normal kidneys.

Advancements in Urology: AUA/JUA Symposium
COI Disclosure Information
Kenichi Kobayashi
I have no COI with regard to our presentation.

Poor performance status is a risk factor for higher detection of Gram positive coccus in stone-related pyelonephritis

19

Hiroki Kawabata, Yuya Iwahashi, Ryusuke Deguchi, Satoshi Muraoka, Takahito Wakamiya, Shimpei Yamashita, Yasuo Kohjimoto, Isao Hara
Department of Urology, Wakayama Medical University, Wakayama, Japan

ABSTRACT

<INTRODUCTION>

We aimed to investigate the detection rate of causative organisms in stone-related pyelonephritis and to compare their distribution according to patient backgrounds.

<METHODS>

We retrospectively identified patients with stone-related pyelonephritis. Clinical data were collected between November 2012 and August 2020 at Wakayama Medical University Hospital, including on patient backgrounds and causative organisms. Patients were categorized by Eastern Cooperative Oncology Group performance status (PS) as the good PS group (0, 1) and the poor PS group (2~4). Bacteria were divided into Gram-positive cocci (GPC) or non-GPC groups and logistic regression analysis was used to examine factors that predict detection of GPC.

<RESULTS>

Seventy-nine patients had stone-related pyelonephritis, 54 (68.4%) in the good PS group and 25 (31.6%) in the poor PS group. In the good PS group, Escherichia coli (67%) was followed by Klebsiella species (9%), while in the poor PS group, Escherichia coli (20%) was followed by Enterococci and Staphylococci (12%). GPC detection rate was significantly higher in the poor PS group than in the good PS group (40.0% vs 14.8%, p=0.016), and multivariate logistic regression analysis showed that poor PS was an independent factor predicting detection of GPC (OR=6.54, p=0.02).

<CONCLUSIONS>

The distribution of the causative organisms in stone-related pyelonephritis was similar to that in common complicated urinary tract infections. Poor PS may be an independent predictor of GPC detection in patients with stone pyelonephritis.

METHODS

- We retrospectively investigated the records of patients from between November 2012 and August 2020 at Wakayama Medical University Hospital, Japan, that had stone-related pyelonephritis.
- We excluded patients for whom bacterial culture tests were not submitted, patients for whom tests were submitted but there was no detection of significant source organisms. We also excluded patients who already had a ureteral stent at the time of onset.
- Patients with ECOG PS 0 or 1 and patients with ECOG PS 2~4 were grouped into good PS and poor PS groups, respectively.

TABLE 1. Patient characteristics

	Total N=79	Good PS n=54	Poor PS n=25	P value
Age, years	75(67-83)	72(62-81)	82(79-88)	<0.01
Sex, n(%) male female	 37(46.8) 42(53.2)	 27(50.0) 27(50.0)	 10(40.0) 15(60.0)	0.40
Diabetes mellitus, n(%)	22(27.8)	16(29.6)	6(24.0)	0.60
Neurogenic bladder, n(%)	7(8.9)	3(5.6)	4(16.0)	0.12
Steroid users, n(%)	5(6.3)	2(3.7)	3(12.0)	0.17
Hydronephrosis, n(%)	63(79.7)	42(77.8)	21(84.0)	0.51
Hospitalization within the last 6 months, n(%)	21(26.6)	10(18.5)	11(44.0)	0.01
Previous use of antibacterial drugs within last 6 months, n(%)	25(31.6)	9(16.7)	16(64.0)	<0.01
Past history of urinary tract infection, n(%)	21(26.6)	8(14.8)	13(52.0)	<0.01
Indwell urethral catherter or ureteral stent within last 6 months, n(%)	11(13.9)	6(11.1)	5(20.0)	0.28

*Continuous variables are shown in "median (quartile)" form.

FIGURE 1. Distribution of causative organisms

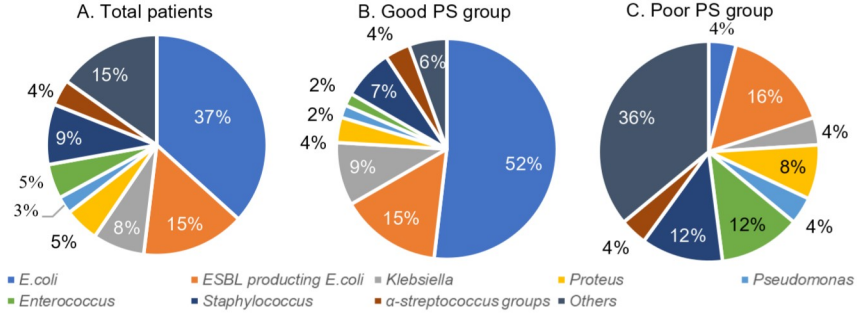

RESULTS

- The 101 patients who did not have a ureteral stent placed at onset were treated for stone-related pyelonephritis. No causative organism could be identified in 22 patients (21.8%), so this study finally included 79 patients. Patient characteristics are shown in TABLE 1.
- The proportion of hospitalized patients and those that had received antibacterial drugs within the previous six months was significantly higher in the poor PS group than in the good PS group (44.0% vs 18.5%, p=0.019; 64.0% vs 16.7%, p＜0.01).
- In the good PS group, two thirds of pathogens were accounted for by E.coli (67%), followed by Klebsiella pneumoniae (9%) (FIGURE 1B). On the other hand, although the detection rate of E.coli was 20%, Enterococcus spp. and Staphylococcus spp. were both detected at the rate of 12% in the poor PS group (FIGURE 1C).
- The detection rate of GPC in the poor PS group was significantly higher than that in the good PS group (40.0% vs 14.8%, p=0.016) (FIGURE 2).
- Multivariate logistic analysis predicting GPC in urine or blood culture demonstrated that poor PS was the only independent factor for detection of GPC (OR=6.54, p=0.02) (TABLE 2).

FIGURE 2. Detection rate of GPC

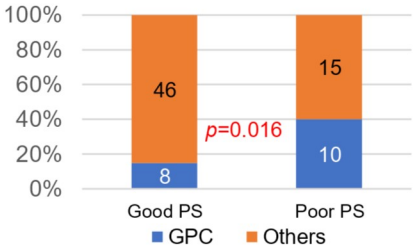

TABLE 2. Predictors of detecting GPC in stone-related pyelonephritis

Predictors	Multivariate analysis OR	95%CI	p value
Age≧75 years	0.42	0.08-1.84	0.26
Hospitalization within the last 6 months,	0.21	0.03-1.20	0.08
Previous use of antibacterial drugs within last 6 months	4.18	0.55-38.9	0.17
Past history of urinary tract infection	0.64	0.11-3.24	0.59
Poor Performance Status	6.54	1.26-42.1	0.02

CONCLUSION

- Patients with good PS had a distribution of causative organisms similar to that of uncomplicated UTI, while more nonspecific causative organisms were detected in patients with poor PS.
- Poor PS was suggested to be an independent predictor of GPC detection.

Advancements in Urology 2024 COI Disclosure Information
Hiroki Kawabata

I have no COI with regard to our presentation

20

Usefulness of 90m Creatinine Clearance Assay in the Evaluation of Renal Function

Ryo Tanaka[1], Soichi Matsumura[1], Shota Fukae[1], Ayumu Taniguchi[2], Shigeaki Nakazawa[1], Kazuaki Yamanaka[1], Yoichi Kakuta[1], Ryoichi Imamura[3], Norio Nonomura[1]

1. Department of Urology, Osaka University Graduate School of Medicine
2. Department of Urology, Juntendo University Urayasu Hospital
3. Department of Urology, Nagasaki University Graduate School of Medicine of Biomedical Sciences

Background

- The accurate assessment of glomerular filtration rate (GFR) as a renal function is very important for both renal transplant donors and recipients.
- The measured GFR (mGFR) using inulin clearance (Cin) is the gold standard for assessing GFR, but it has disadvantages associated with the administration of exogenous substances.
- Twenty-four-hour creatinine clearance (24hCCr) and the estimated GFR(eGFR) calculated using serum creatinine levels is widely used for GFR assay using endogenous substances, but the former requires long-time urine storage and the latter is not accurate enough.
- The development of a simple, accurate, and minimally invasive method of measuring GFR is desired.
- We defined 90min CCr (90mCCr) as CCr measured by the 30 min x 3 times method.

methods	merit	demerit
mGFR (Inulin clearance)	Very accurate **(gold standard)**	Administration of exogenous substances
24hr CCr	Only endogenous substances	Long-time urine storage
eGFR(JSN2009)	Simple(only blood collection)	Not accurate enough

"Without exogenous substances", "Short-time", "Accurate" new method :90mCCr

Aim

- The aim of this study is to investigate the usefulness of a new CCr assay that can be performed in a short time and Without exogenous substances.

Conclusion

- The Adjusted 90mCCr is useful new method of assessing renal function.

Summary of result

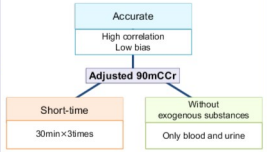

Method

1. Measurement of mGFR and 90mCCr

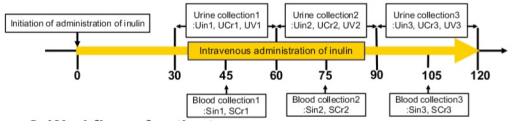

$$\frac{UCr1\times UV}{SCr1}\times\frac{1.73}{BSA}=CCr1,\ \frac{CCr1+CCr2+CCr3}{3}=\textbf{90mCCr}$$

$$\frac{Uin1\times UV1}{Sin1}\times\frac{1.73}{BSA}=Cin1,\ \frac{Cin1+Cin2+Cin3}{3}=\textbf{mGFR}$$

2. Workflow of patients

Total cohort:434 cases
Pre-donation donor: 293 cases
Post-donation donor: 53cases
Post-transplant recipients: 88cases

② : ①

Study cohort 289 cases

Validation cohort 145 cases

1. Total cohort

✓We measured 90min CCr (90mCCr) and mGFR.
✓The correlation between 90mCCr and mGFR was evaluated by single regression analysis.
✓ The bias and accuracy of 90mCCr for mGFR were calculated.

2. Study and Validation cohort

✓We divided total cohort 2:1 into study and validation cohort.
✓We established a correction equation for 90mCCr to mGFR using single regression analysis in study cohort
✓The correlation and bias of the Adjusted 90mCCr with mGFR was evaluated in Validation cohort.

Result

1. Patients' characteristics

	Total cohort	Study cohort	Validation cohort	P value
Gender (male/female)	193/241	131/158	62/83	0.68
Age (years old)	61(22-85)	60(23-85)	62(22-82)	0.25
Height (m)	1.61(1.39-1.93)	1.60(1.39-1.93)	1.61(1.39-1.85)	0.94
Body weight (kg)	60(34-91)	60(34-91)	59.8(34-87)	0.58
BSA (m^2)	1.63(1.19-2.17)	1.63(1.19-2.17)	1.61(1.20-2.05)	0.66
Patient type (Pre-donor/Post-donor/Recipient)	293/53/88	195/36/58	98/17/30	0.97
mGFR (mL/min/1.73m^2)	68.7(16.8-137.6)	68.5(16.8-128.9)	69.2(21.2-137.6)	0.94
eGFR(JSN2009) (mL/min/1.73m^2)	69.1(24.8-123.1)	68.6(27.9-123.1)	70.6(24.8-105.5)	0.94
90mCCr (mL/min/1.73m^2)	98.6(25.9-214.0)	99.7(25.9-214.0)	96.7(33.9-172.4)	0.95

BSA: Body surface area , eGFR: estimated glomerular filtration rate — median(range)

2. The distribution of 90mCCr and mGFR in total cohort

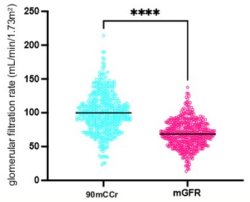

90mCCr	98.6(25.9-214.0)
mGFR	68.7(16.8-137.6)
P value	<0.001

median(range)

90mCCr level was significantly higher than mGFR level.

3. The correlation between 90mCCr and mGFR in total cohort

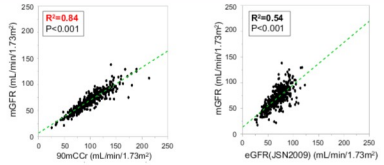

90mCCr showed a strong correlation with mGFR.

4. The correlation between 90mCCr and mGFR by patient groups

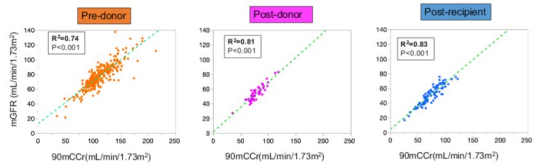

In all patient groups, 90mCCr showed a good correlation with mGFR.

4. The bias of 90mCCr with mGFR in total cohort

Bland-Altman plots of 90mCCr and eGFR for mGFR in total cohort

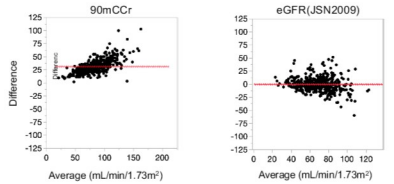

	Bias	95%CI low	95%CI high
90mCCr	30.9	29.7	32.1
eGFR	-0.65	-1.92	0.63

The bias of 90mCCr on mGFR was high.

5. The correction of 90mCCr for mGFR in study cohort

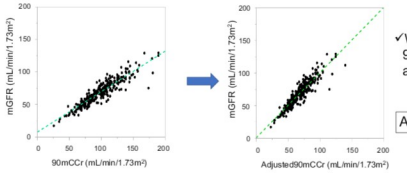

✓We established a correction equation for 90mCCr to mGFR using single regression analysis in study cohort.

Adjusted 90mCCr=7.10+0.62×90mCCr

6. Adjusted 90mCCr and mGFR in Validatoion cohort

The distribution of Adjusted 90mCCr for mGFR

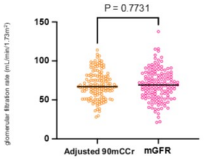

The correlation of Adjusted 90mCCr for mGFR

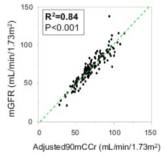

Bland-Altman plots of Adjusted 90mCCr and eGFR for mGFR

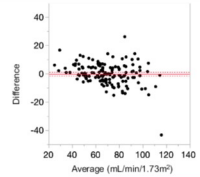

Bias(95% CI) -0.19(-1.45~1.08)

waterfall plots of Adjusted 90mCCr for mGFR

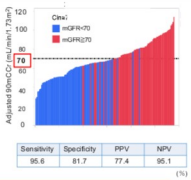

Sensitivity	Specificity	PPV	NPV
95.6	81.7	77.4	95.1

(%)

Adjusted 90mCCr showed a strong correlation and low bias with mGFR.

21

id020

The MAG3 renal scintigraphy performed on the first postoperative day predicts early postoperative renal function recovery

Shigeaki Nakazawa, Soichi Matsumura, Shota Fukae, Ryo Tanaka, Kazuaki Yamanaka, Yoichi Kakuta, Norio Nonomura
Osaka University Graduate School of Medicine, Department of Urology

Background

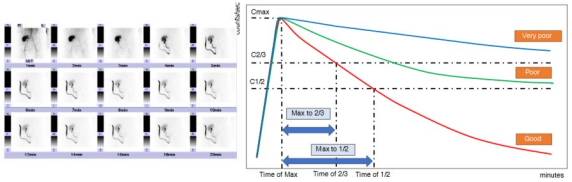

- ✓ At our institution, MAG3 renal scintigraphy on postoperative day 1 has been performed to confirm that the vascular anastomosis is fully functional.
- ✓ If MAG3 is detected throughout the kidney, it indicates that the entire kidney is perfused without any blood flow obstruction.
- ✓ However, we have noticed different excretion patterns in different cases.
- ✓ We hypothesized that MAG3 renal scintigraphy on postoperative day 1 would reflect the degree of acute tubular necrosis and predict early recovery of renal function after transplantation.
- ✓ And identifying factors involved in differences in MAG3 renal might scintigraphy contribute to a rapid improvement in renal function.

Methods

・The maximum detection speed is defined as Cmax, 2/3 as C2/3, and half as C1/2.
・The time to reach Cmax, C2/3, and C1/2 are defined as Tmax, T2/3, and T1/2, respectively.
・Define the time from Tmax to T2/3 as Max to 2/3 and the time from Tmax to T1/2 as Max to 1/2.

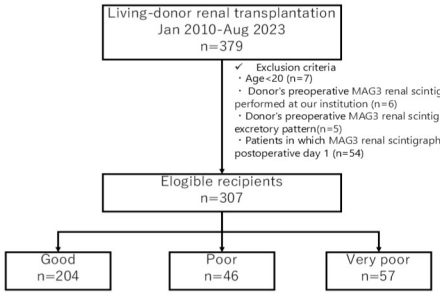

Patients were divided into 3 groups:
good group; patients who could reach C1/2,
poor group; patients who could reach C2/3 but not C1/2,
very poor group ; patients who could not reach C2/3.

Aim

The objective was this study to determine whether MAG3 could predict early recovery of renal function after transplantation and to identify factors associated with it.

Conclusion

MAG3 renal scintigraphy on postoperative day 1 helps predict improvement in postoperative graft function.
Risk factor influencing excretion patterns in MAG3 renal scintigraphy was TIT.

Results

Patient characteristics

Characteristic	good, N = 204[1]	poor, N = 46[1]	very poor, N = 57[1]	p-value2
Recipient gender				0.03
F	87 (42.6%)	12 (26.1%)	16 (28.1%)	
M	117 (57.4%)	34 (73.9%)	41 (71.9%)	
Recipient age at TPL (yr)	49.0 (38.0, 60.0)	52.5 (44.2, 61.8)	47.0 (40.0, 59.0)	0.32
Recipient age at RRT (yr)	46.0 (35.0, 56.0)	49.5 (40.2, 59.0)	42.0 (36.5, 51.5)	0.16
Donor gender				0.69
F	129 (63.2%)	26 (56.5%)	36 (63.2%)	
M	75 (36.8%)	20 (43.5%)	21 (36.8%)	
Donor age at TPL (yr)	59.0 (51.0, 67.0)	63.0 (56.0, 67.5)	63.0 (54.0, 73.0)	0.009
Donor mGFR(ml/min/1.73m2)	93.2 (83.9, 106.6)	88.8 (79.7, 97.2)	94.0 (85.7, 102.5)	0.11
Gender mismatch				0.069
F to M	91 (44.6%)	25 (54.3%)	26 (45.6%)	
M to F	49 (24.0%)	11 (23.9%)	6 (10.5%)	
match	64 (31.4%)	10 (21.7%)	25 (43.9%)	
Preemptive	39 (19.1%)	7 (15.2%)	13 (22.8%)	0.62
Preoperative DSA positive	9 (4.4%)	1 (2.2%)	4 (7.0%)	0.5
ABO blood type compatibility				0.96
compatible	133 (65.2%)	29 (63.0%)	37 (64.9%)	
incompatible	71 (34.8%)	17 (37.0%)	20 (35.1%)	
Recipient DM	56 (27.7%)	12 (26.7%)	10 (17.9%)	0.32
Recipient history of smoking	78 (38.8%)	16 (34.8%)	27 (47.4%)	0.38
Recipient BMI (kg/m^2)	21.2 (19.0, 24.1)	21.4 (19.7, 24.3)	22.8 (20.1, 26.3)	0.033
Donor BMI (kg/m^2)	22.4 (20.6, 24.5)	23.2 (21.9, 24.9)	22.9 (21.5, 24.9)	0.41
Donor BMI / Recipient BMI	1.1 (0.9, 1.2)	1.0 (0.9, 1.2)	1.0 (0.9, 1.1)	0.65
WIT (sec)	120.0 (104.5, 147.0)	116.0 (100.0, 153.8)	130.0 (107.0, 159.5)	0.28
TIT (min)	84.0 (71.2, 98.0)	96.5 (80.5, 111.9)	94.0 (75.8, 110.0)	0.013
Arterial reconstruction	8 (4.7%)	3 (7.5%)	6 (12.8%)	0.12
Aretrial anastomosis method				0.94
end-to-end	42 (25.9%)	10 (25.0%)	11 (23.4%)	
end-to-side	120 (74.1%)	30 (75.0%)	36 (76.6%)	
Arterial anastomosis site				0.98
external illiac artery	100 (62.1%)	23 (57.5%)	29 (61.7%)	
internal illiac artery	51 (31.7%)	14 (35.0%)	15 (31.9%)	
common illiac artery	10 (6.2%)	3 (7.5%)	3 (6.4%)	
FK trougn concentration at POD1 (ng/mL)	11.5 (7.3, 20.6)	9.9 (7.9, 19.2)	11.8 (7.5, 26.9)	0.58

1n (%); Median (IQR)
2Pearson's Chi-squared test; Kruskal-Wallis rank sum test; Fisher's exact test

2. Parameter of MAG3 renal scintigraphy

Characteristic	good, N = 204[1]	poor, N = 46[1]	very poor, N = 57[1]	p-value[2]
Time of Cmax	2.00 (1.67, 2.67)	3.75 (2.88, 5.50)	6.59 (4.00, 13.47)	<0.001
Time of C2/3	5.36 (4.27, 6.95)	14.45 (11.72, 17.32)	NA (NA, NA)	<0.001
Time of C1/2	9.60 (6.89, 12.60)	NA (NA, NA)	NA (NA, NA)	
Time from Cmax to C2/3	3.27 (2.49, 4.40)	9.71 (7.86, 13.23)	NA (NA, NA)	<0.001
Time from Cmax to C1/2	7.31 (4.99, 10.02)	NA (NA, NA)	NA (NA, NA)	

1n (%); Median (IQR)
2Pearson's Chi-squared test; Kruskal-Wallis rank sum test; Fisher's exact test

3. Clinical course of postoperative eGFR

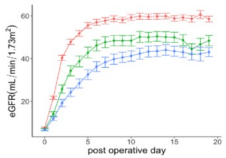

4. Clinical course of postoperative FK trough concentration

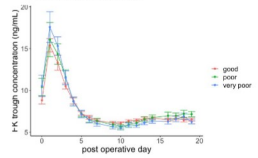

5. Multiple regression analysis to identify risk factors

	95% CI	p-value
Recipient BMI	[-0.02, 0.08]	0.206
Recipient gender (M)	[0.00, 0.82]	0.058
Recipient age at TPL	[-0.02, 0.00]	0.192
Donor age at TPL	[0.00, 0.03]	0.106
TIT	[0.00, 0.01]	0.024

Advancements in Urology 2024
COI Disclosure Information
Shigeaki Nakazawa

I have no COI with regard to our presentation